DSMC MULTICOMPONENT AEROSOL DYNAMICS: SAMPLING ALGORITHMS AND AEROSOL PROCESSES

A Dissertation
presented to
the Faculty of the Graduate School
at the University of Missouri-Columbia

In Partial Fulfillment
of the Requirements for the Degree

Doctor of Philosophy

---

by
Geethpriya Palaniswaamy

Dr. Sudarshan K. Loyalka Dissertation Supervisor

August, 2007

The undersigned, appointed by the Dean of the Graduate School, have examined the dissertation entitled

DSMC MULTICOMPONENT AEROSOL DYNAMICS:
SAMPLING ALGORITHMS AND AEROSOL PROCESSES

presented by Geethpriya Palaniswaamy

a candidate for the degree of Doctor of Philosophy

and hereby certify that in their opinion it is worthy of acceptance

_____
Dr. Sudarshan K. Loyalka, Nuclear Science and Engineering Institute

_____
Dr. Robert V. Tompson Jr., Nuclear Science and Engineering Institute

_____
Dr. Tushar K. Ghosh, Nuclear Science and Engineering Institute

_____
Dr. Mark A. Prelas, Nuclear Science and Engineering Institute

_____
Dr. Dabir S. Viswanath, Department of Chemical Engineering

ACKNOWLEDGEMENTS

I express my deep gratitude and thanks to my advisor, **Dr. Sudarshan K. Loyalka** for his valuable guidance, patience, encouragement and his suggestions at all times during this work.

I would like to thank **Profs. Robert Tompson**, **Mark Prelas**, **Tushar Ghosh**, and **Dabir Viswanath** for their comments on improving this work and their patience in reviewing this work. There are many others in the nuclear engineering department whose help I have appreciated.

I would also like to extend my thanks to the Nuclear Energy Education and Research Program and the **U. S. Department of Energy** for supporting this study under the grant, ***"Nuclear Aerosols: Direct Simulation and Elucidation of Role of Multiple Components, Radioactivity, Charge, Shape and Spatial Inhomogeneity"***.

I would like to thank all my friends for their support and help. Also, I would like to extend my thanks to my parents and my family for their support, inspiration and motivation at all times.

TABLE OF CONTENTS

LIST OF FIGURES

LIST OF TABLES

ABSTRACT

The post-accident nuclear reactor primary and containment environments can be characterized by high temperatures and pressures, and fission products and nuclear aerosols. These aerosols evolve via natural transport processes as well as under the influence of engineered safety features. These aerosols can be hazardous and may pose risk to the public if released into the environment. Computations of their evolution, movement and distribution involve the study of various processes such as coagulation, deposition, condensation, etc., and are influenced by factors such as particle shape, charge, radioactivity and spatial inhomogeneity. These many factors make the numerical study of nuclear aerosol evolution computationally very complicated. The focus of this research is on the use of the Direct Simulation Monte Carlo (DSMC) technique to elucidate the role of various phenomena that influence the nuclear aerosol evolution.

In this research, several aerosol processes such as coagulation, deposition, condensation, and source reinforcement are explored for a multi-component, aerosol dynamics problem in a spatially homogeneous medium. Among the various sampling algorithms explored the Metropolis sampling algorithm was found to be effective and fast. Several test problems and test cases are simulated using the DSMC technique. The DSMC results obtained are verified against the analytical and sectional results for appropriate test problems. Results show that the assumption of a single mean density is not appropriate due to the complicated effect of component densities on the aerosol processes. The methods developed and the insights gained will also be helpful in future research on the challenges associated with the description of fission product and aerosol releases.

1. INTRODUCTION

1.1 Background

Nuclear aerosols can originate from severe core damage in light water reactors, core disruptive accidents in fast reactors, nuclear accidents during nuclear material transport, at waste disposal sites, or explosions [1 - 6]. These nuclear aerosols contain several radioactive elements in their composition. Tables 1 and 2 show the radionuclides released into the containment as aerosols during accidents in the pressurized water reactor (PWR) and boiling water reactor (BWR), respectively [7]. The post-accident reactor environment can be characterized to be in a highly non-equilibrium condition with very high temperatures and pressures, and nuclear aerosol (particle) formation. These aerosols evolve under natural transport processes as well as under the influence of engineered safety features. Such aerosols can be hazardous for the equipment inside the reactor, and when leaked to the environment, pose potential risks to the public [8 - 12]. Hence, the origin, movement and distribution of these aerosols need to be studied and controlled. Computations involved with the predictions of the evolution of these aerosols, however, is complicated, and our purpose is to use the Direct Simulation Monte Carlo (DSMC) technique to elucidate the role of various physical phenomena that influence the aerosol evolution, and eventually help develop a production computer program.

Table 1: PWR releases into containment.* [7]

	Gap Release	Early In-Vessel	Ex-Vessel	Late In-Vessel
Duration (Hours)	0.5	1.3	2.0	10.0
Noble Gases	0.05	0.95	0	0
Iodine	0.05	0.35	0.29	0.07
Cesium	0.05	0.25	0.39	0.06
Tellurium	0	0.15	0.29	0.025
Strontium	0	0.03	0.12	0
Barium	0	0.04	0.10	0
Ruthenium	0	0.008	0.004	0
Cerium	0	0.01	0.02	0
Lanthanum	0	0.002	0.015	0

* Values shown are fractions of core inventory.

Table 2: BWR releases into containment.* [7]

	Gap Release	Early In-Vessel	Ex-Vessel	Late In-Vessel
Duration (Hours)	1.0	1.5	3.0	10.0
Noble Gases	0.05	0.95	0	0
Iodine	0.05	0.22	0.37	0.07
Cesium	0.05	0.15	0.45	0.03
Tellurium	0	0.11	0.38	0.01
Strontium	0	0.03	0.24	0
Barium	0	0.03	0.21	0
Ruthenium	0	0.007	0.004	0
Cerium	0	0.009	0.01	0
Lanthanum	0	0.002	0.01	0

* Values shown are fractions of core inventory.

There had been several computer codes like ABC, AEROSIM, ASTD, CONTAIN, HAARM, MELCOR, PARIDESKO, RAFT, SCDAP, TRAP-MELT, VICTORIA, and many more that model accident progression in reactor containments [12 - 19]. These computer codes use various methods such as the finite elements method, the moments method, the analytical method, the sectional method, and other numerical methods to simulate the aerosol dynamics. Also, these codes work on several assumptions that compromise the collisional physics. Figure 1 shows the modules present in one such code – CONTAIN [17], emphasizing the three basic phenomenological areas and the inter-coupling between the modules. The module on aerosol dynamics called MAEROS [13, 17] is based on the sectional method.

The motivation behind this work is to develop a production computer program which simulates the evolution and dynamics of multi-component aerosols with minimal assumptions without compromising the collisional physics.

The complexity involved with aerosol dynamics increases with the inclusion of various properties such as size, shape, charge, radioactivity and spatial inhomogeneity. Also, particles in suspension undergo various processes such as condensation, coagulation, deposition and evaporation. The set of equations used to describe the aerosol behavior mentioned above is non-linear which makes the problem of multi-component aerosol dynamics and computations more complicated.

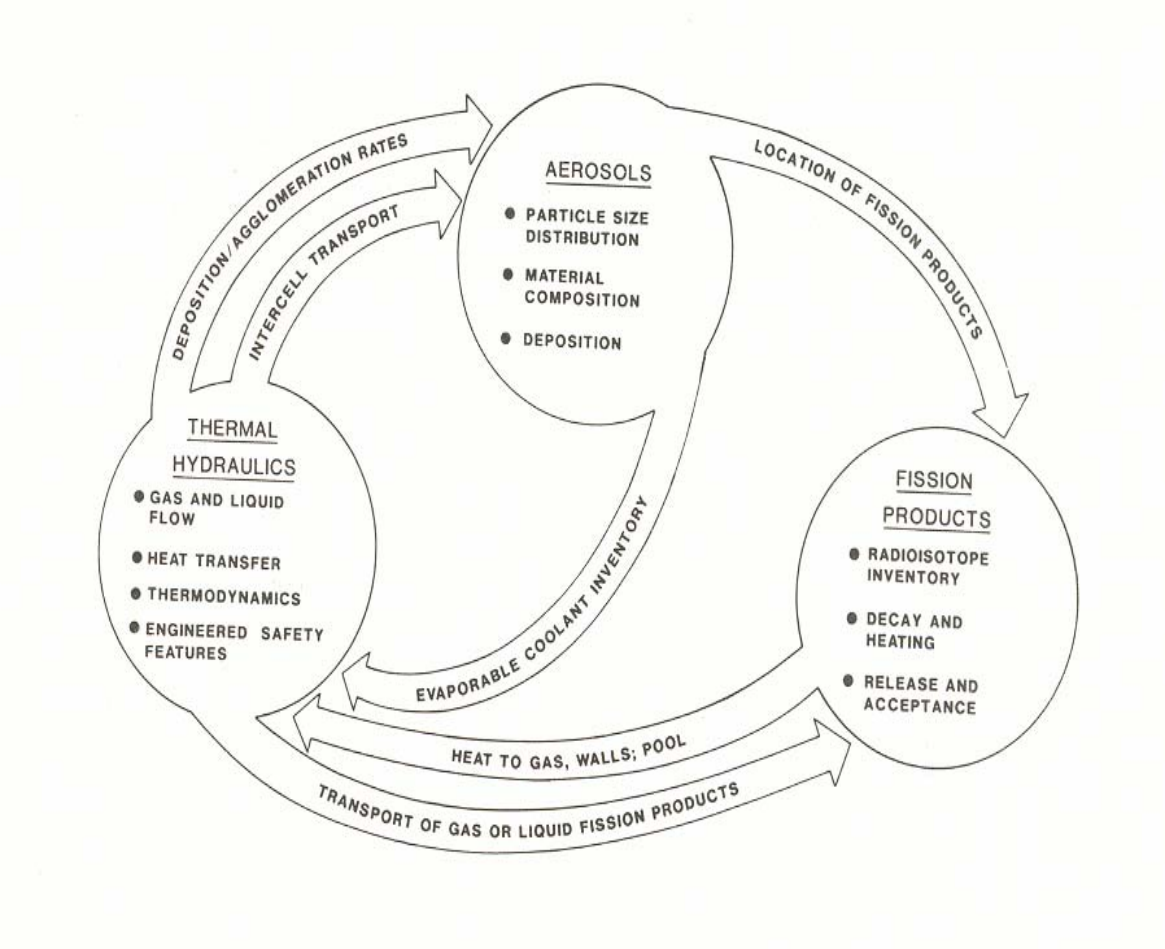

Figure 1: Schematic diagram of the CONTAIN code. [17]

Loyalka [20] proposed the use of the DSMC technique for nuclear aerosols and showed that, for the coagulation model involving two component aerosols with the same component density, the results agreed well with those obtained from both sectional and analytical methods. Rangaraj and Loyalka [21] extended computations to multiple component aerosols (with different component densities) undergoing pure Brownian coagulation. They found that the sectional method used in MAEROS [13, 17] could not describe such aerosols well. Palaniswaamy and Loyalka [22] further extended the study to multi-component aerosols with different component densities and also, included several coagulation mechanisms such as Brownian, gravitational and turbulent coagulation kernels as well as the source reinforcement process.

1.2 Objective and Organization

In this research, the study on aerosol dynamics is further explored to include multiple components with different component densities and several aerosol processes such as coagulation, deposition, condensation, and source reinforcement. Several collisional sampling algorithms – the No Time Counter (NTC) method [23], the Metropolis sampling [24], direct sampling and modified direct sampling algorithms are explored. From the results observed, it is concluded that the Metropolis sampling algorithm gives better results and also reduces the computation time significantly. This has helped in increasing the initial particle population for the simulation from 1000 to more than 100,000 [25]. Currently, with better computer resources (2 GB RAM), a higher particle population of 4 million is achieved.

Several single component aerosol dynamics test problems were simulated using the DSMC technique. The DSMC results are compared against those obtained using the analytical method and they agree well with the analytical results. Additionally, multi-component aerosol dynamics problem with the same component density is simulated using both the DSMC technique and the sectional method for several test problems and the results compared. One important observation made is that the assumption of a single mean density is not appropriate due to the complicated effect of different component densities on the aerosol processes [26].

The outline of this work is described as follows. Chapter II presents some of the recent works and earlier results obtained in this area. It starts with a discussion on the aerosol dynamics and the general dynamic equation. It also briefly describes the coagulation process and continues with the recent works and results obtained.

Chapter III describes the collisional sampling algorithms explored, the test problems simulated and their results and conclusions. Chapter IV describes the aerosol deposition and source reinforcement processes, analytical solutions, test problems, the DSMC implementation, and results. Chapter V describes the aerosol condensation process, analytical solutions, test problems, the DSMC implementation, and results. Chapter VI summarizes the results and also discusses the conclusions obtained from the study.

2. REVIEW OF THE RECENT WORKS

2.1 Aerosol Dynamics and the General Dynamic Equation (GDE)

The aerosol behavior involves several factors such as particle size, composition, shape, charge, spatial inhomogeneities, environmental conditions, and thermal hydraulics that influence the aerosol evolution process. This complex behavior of aerosols is expressed mathematically using general dynamic equations (GDEs). In general, the GDE is expressed using the number of aerosol particles per cubic meter, $n(\boldsymbol{v},\boldsymbol{m},t)$ of a species, p ($1 \le p \le$ N), contained in a volume varying from v_p to $v_p + dv_p$, with mass ranging from m_p to $m_p + dm_p$. The aerosol GDE for a well-mixed, spherical, multi-species aerosol is given as [11, 27]:

$$\begin{aligned}\frac{\partial}{\partial t}n(\boldsymbol{v},\boldsymbol{m},t)+R(\boldsymbol{v},\boldsymbol{m},t)n(\boldsymbol{v},\boldsymbol{m},t)+\sum_{p=1}^{N}\frac{\partial}{\partial v_p}\left[I_p(\boldsymbol{v},\boldsymbol{m},t)n(\boldsymbol{v},\boldsymbol{m},t)\right]\\ =\frac{1}{2}\int_0^\infty d\boldsymbol{u}\int_0^\infty d\boldsymbol{w}\int_0^\infty d\boldsymbol{q}\int_0^\infty d\boldsymbol{s}\; n(\boldsymbol{u},\boldsymbol{q},t)n(\boldsymbol{w},\boldsymbol{s},t)K(u,q\,|\,w,s)\\ \times\prod_{p=1}^{N}\delta(v_p-u_p-w_p)\delta(m_p-q_p-s_p)\\ -n(\boldsymbol{v},\boldsymbol{m},t)\int_0^\infty d\boldsymbol{u}\int_0^\infty d\boldsymbol{q}K(u,q\,|\,v,m)n(\boldsymbol{u},\boldsymbol{q},t)+S(\boldsymbol{v},\boldsymbol{m},t)\end{aligned} \tag{2-1}$$

where $q=\sum_{p=1}^{N}q_p$ and $s=\sum_{p=1}^{N}s_p$

In Eq. (2-1), $R(\boldsymbol{v},\boldsymbol{m},t)$ is the removal rate via deposition mechanisms like diffusion, settling, thermophoresis, sprays, etc. (s^{-1}), $I_p(\boldsymbol{v},\boldsymbol{m},t)$ is the condensation rate ($m^3\ s^{-1}$), and $K(u,q\,|\,w,s)$ is the coagulation kernel for particles of total volumes (u), and masses (q), coalescing with particles of total volumes (w), and masses (s) ($m^3\ s^{-1}$). The delta functions in Eq. (2-1) help to ensure conservation of volume and mass in a collision [11, 28, 29]. $S(\boldsymbol{v},\boldsymbol{m},t)$ refers the source reinforcement term ($m^{-3}\ s^{-1}$). It needs to be mentioned here that a spatially homogeneous medium is being considered in this study. For further details on Eq. (2-1), the reader is referred to the work of Williams and Loyalka [11].

As can be seen from equation (2-1), the GDE for aerosols is an integro-differential equation and hence, becomes very complicated to solve because of the dynamic behavior of the aerosols. There have been a number of techniques such as analytical method, numerical method, finite element method, method of moments, sectional method, etc., proposed to solve the GDE and study the aerosol dynamics problem. A review on these techniques can be found in Williams and Loyalka [11].

In 1976, Bird [30] proposed the DSMC technique for rarefied gas dynamics in which the molecular motion was simulated through a splitting technique. Loyalka [20] proposed the use of the DSMC technique for the study of nuclear aerosols. He simulated a two-component, same component density problem. A brief description of the problem, recent works and their results are presented in the following sections.

2.2 Two Component, Same Component Density Problem

For this problem, a computer program was developed to explore the coagulation of multi-component particles in spatially homogeneous systems. The program was run for a two component test problem which is expressed in a non-dimensional form as:

$$\frac{\partial n\ (v_1, v_2, t)}{\partial t} = \frac{1}{2} K_0 \int_0^{v_1} du_1 \int_0^{v_2} du_2\ n\ (u_1, u_2, t)\, n\ (v_1 - u_1, v_2 - u_2, t) - K_0 n\ (v_1, v_2, t) \int_0^{\infty} du_1 \int_0^{\infty} du_2 n\ (u_1, u_2, t) \tag{2-2}$$

subject to the initial condition:

$$n_0(v_1, v_2) = \frac{N_0}{v_{10} v_{20}} \exp\left\{ -\left(\frac{v_1}{v_{10}} + \frac{v_2}{v_{20}} \right) \right\} \tag{2-3}$$

where N_0 is the number of initial particles, K_0 is constant and v_{10} and v_{20} are the average initial volumes of the particles. Using a transform technique,

$$n(v_1, v_2, t) = \frac{N_0}{v_{10} v_{20} (1+\tau)^2} \exp\left\{ -\left(\frac{v_1}{v_{10}} + \frac{v_2}{v_{20}} \right) \right\} I_0 \left\{ 2 \left[\frac{\tau v_1 v_2}{(1+\tau) v_{10} v_{20}} \right]^{1/2} \right\} \tag{2-4}$$

where $\tau = K_0 N_0 t / 2$ and $I_0\ (x)$ is a modified Bessel function. The sectional distributions, useful for comparisons later, are computed from:

$$\begin{aligned} n_l(t) &= \int_0^{\infty} dv_1 \int_0^{\infty} dv_2 \varepsilon^{(l)}(v_1, v_2) n(v_1, v_2, t), \\ Q_{l,k}(t) &= \int_0^{\infty} dv_1 \int_0^{\infty} dv_2 \varepsilon^{(l)}(v_1, v_2) v_k n(v_1, v_2, t) \end{aligned} \tag{2-5}$$

where $k = 1,2$, and $\varepsilon^{(l)}(v_1,v_2) = 1$ for $v^{(l-1)} \le v_1 + v_2 < v^{(l)}$; and 0 otherwise.

All the programming was carried out in a single framework and the analytical and direct simulation results obtained were compared as shown in figs. 2 and 3.

For illustration, 15 sections were defined by the geometric distribution as:

$$v^{(0)} = 0, \qquad v^{(1)} = (v_{10} + v_{20})/8;$$
$$v^{(l)} = 2v^{(l-1)}, \quad l = 2,..14; \qquad v^{(15)} = 10v^{(14)}$$

where $N_0 = 10000,\ K_0 = 1.0,\ v_{10} = 1.0$ and $v_{20} = 1.5$.

The darker portions in the component mass distributions in figs. 2 and 3 specify the mass for component 1, while the lighter portions indicate the mass of component 2. Component mass and number of particles are plotted against the various sections (bins).

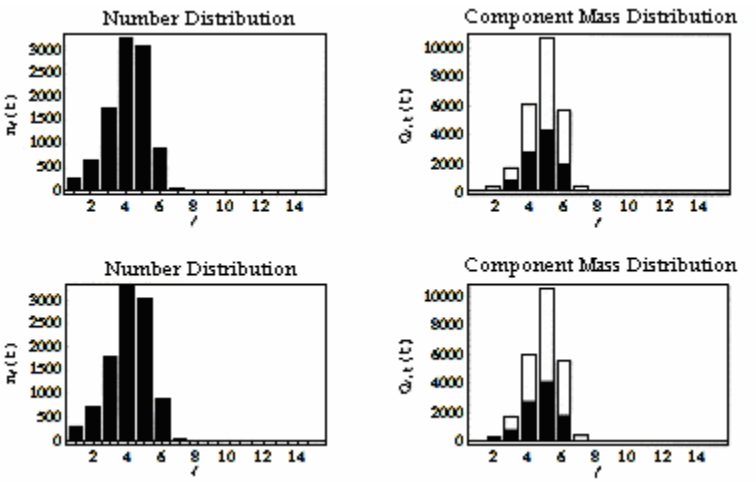

Figure 2: Initial particle number and component mass distributions.

(Top row: Analytical method. Bottom row: DSMC technique).

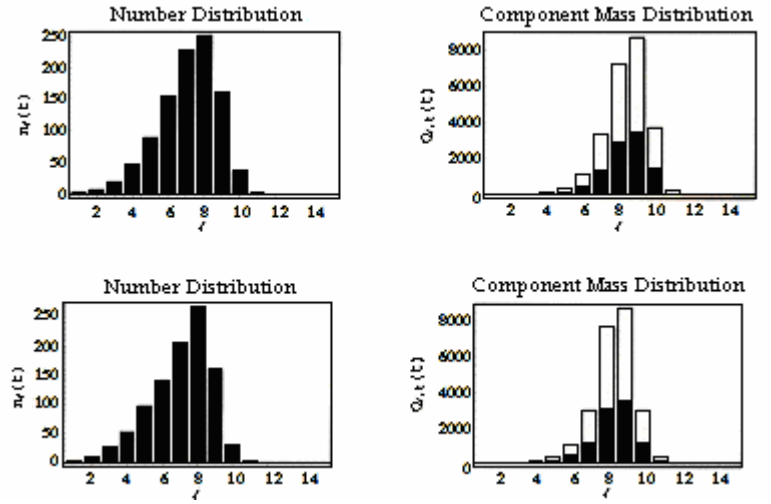

Figure 3: Particle number and component mass distributions after 9,000 collisions.

(Top row: Analytical method. Bottom row: DSMC technique).

2.3 Two Component, Different Component Density Problem

Rangaraj and Loyalka [21] extended the work to multiple component aerosols undergoing pure Brownian coagulation. They also benchmarked the DSMC technique with the sectional technique as described in the MAEROS user manual [13].

For a two component aerosol problem, Rangaraj and Loyalka [21] considered the following initial condition expressed using the component mass as:

$$n_0(m_1, m_2) = \frac{N_0}{m_{10} m_{20}} \exp\left\{-\left(\frac{m_1}{m_{10}} + \frac{m_2}{m_{20}}\right)\right\} \tag{2-6}$$

where N_0 is the number of initial particles (= 1000) and m_{10} and m_{20} are the component masses (taken as 1.0 and 1.5 respectively). The test conditions considered were:

Test Condition 1: ρ_1 = 1000 kg m^{-3}; ρ_2 = 1000 kg m^{-3}.

Test Condition 2: ρ_1 = 1000 kg m^{-3}; ρ_2 = 10,000 kg m^{-3}.

The results obtained using the DSMC approach was compared against those of the sectional approach and the sectional results (fig. 4) matched well with the DSMC results (fig. 5) for a two-component model with constant densities – test condition 1. However, the sectional method does not account for different component densities; hence, only the DSMC results were obtained for a two-component, different component density problem – test condition 2, and are shown in fig. 6.

Here too, the darker portions in the component mass distributions in figs. 4 - 6 specify the mass of component 1, while the lighter portions indicate the mass of component 2.

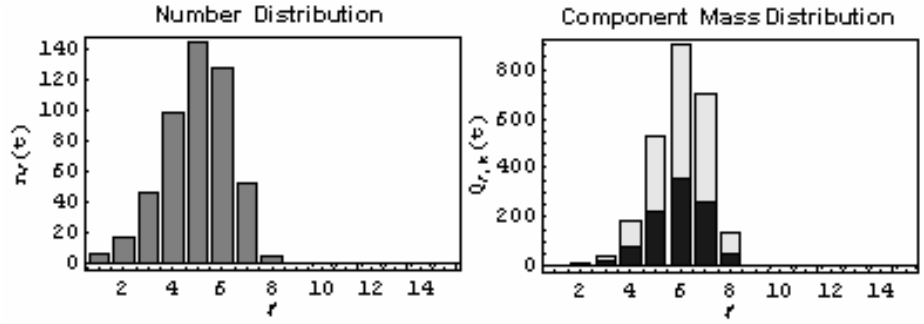

Figure 4: Particle number distribution (left) and component mass distribution (right) for test condition 1 (ρ_1 = 1000 kg m^{-3}; ρ_2 = 1000 kg m^{-3}), using sectional method.

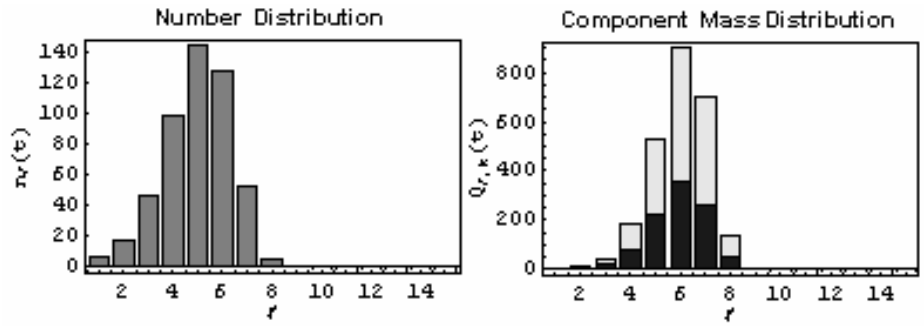

Figure 5: Particle number distribution (left) and component mass distribution (right) for test condition 1 (ρ_1 = 1000 kg m^{-3}; ρ_2 = 1000 kg m^{-3}), using the DSMC technique.

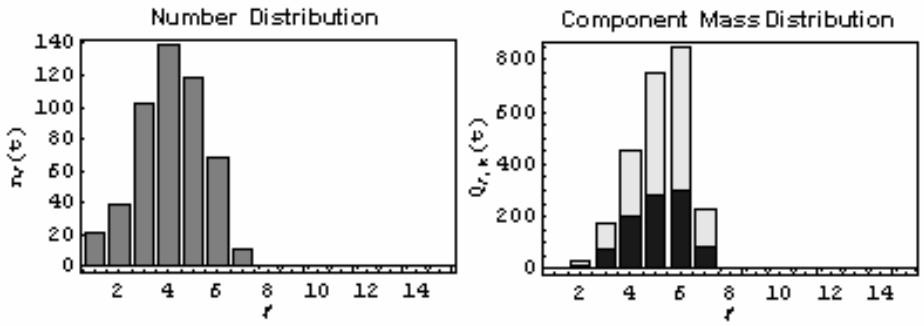

Figure 6: Particle number distribution (left) and component mass distribution (right) for test condition 2 (ρ_1 = 1000 kg m^{-3}; ρ_2 = 10,000 kg m^{-3}), using the DSMC technique.

2.4 Aerosol Coagulation

Coagulation is a term used to describe the process of collision of two particles resulting in adhesion (or fusion) to produce a larger particle. Collision between two particles occurs due to several factors – Brownian motion of particles, gravitational and turbulent effects on particles, acoustic effects and so on. Here we consider models for Brownian, gravitational and turbulent coagulation kernels, where Brownian coagulation accounts for coagulation due to the free random motion of the particles in a medium; gravitational kernel accounts for two particles coming in contact with each other due to the gravitational effects; and turbulent kernel accounts for the collision of two particles due to the turbulence effect in the fluid motion [31 - 33]. In this work, the expressions used for the three coagulation kernels are as specified in the MAEROS user manual [13] although several improved expressions of the kernels are now available. The following three equations are used in this work [11, 27].

$$\beta_{Brownian} = \frac{2\pi(D_i + D_j)(\gamma_i d_i + \gamma_j d_j)}{\left(\frac{d_i + d_j}{d_i + d_j + 2\sqrt{g_i^2 + g_j^2}} + \frac{8\,(D_i + D_j)}{\sqrt{V_i^2 + V_j^2}\,(d_i + d_j)} \right)} \tag{2-7}$$

$$\beta_{gravitational} = \varepsilon \frac{\pi}{4} (\gamma_i d_i + \gamma_j d_j)^2 \left| V_{T_i} - V_{T_j} \right| \tag{2-8}$$

$$\beta_{turbulence} = \sqrt{\frac{\pi\ \varepsilon_T}{120\ \upsilon} (\gamma_i d_i + \gamma_j d_j)^6 + \frac{0.00162\ \rho_g^{1/2} \varepsilon_T^{3/2}}{\eta^{5/2}} (\gamma_i d_i + \gamma_j d_j)^2 \left| \frac{\rho_{p\,i}\ C_i\ d_i^2}{\chi_i} - \frac{\rho_{p\,j} C_j d_j^2}{\chi_j} \right|^2} \tag{2-9}$$

where:

$$D_i = \frac{kTC_i}{3\pi d_i \eta \chi_i}$$

$$C_i = 1 + Kn_i\ [1.37 + 0.4\ \exp\ (-1.1/Kn_i)]$$

$$Kn_i = 2\lambda / d_i$$

$$g_i = \frac{1}{3D_i\ell_i}[(d_i + \ell_i)^3 - (d_i^2 + \ell_i^2)^{3/2}] - d_i$$

$$\ell_i = \frac{8d_i}{\pi V_i} \qquad V_i = \sqrt{\frac{8kT}{\pi m_i}}$$

$$V_{T_i} = \frac{\rho_{pi}\ g\ d_i^2\ C_i}{18\ \eta\ \chi_i}$$

$$\varepsilon = \frac{d_i^2}{(d_i + d_j)^2}; \quad d_i < d_j$$

$$\varepsilon = \frac{d_j^2}{(d_i + d_j)^2}; \quad d_i > d_j$$

The subscripts, i and j, denote the i^{th} and j^{th} particle with mass represented by m (kg). Kn refers to the Knudsen number, λ is the mean free path (m), d is the particle diameter (m), T is the absolute temperature (K), k is the Boltzmann constant (J K^{-1}), η is the gas viscosity (kg m^{-1} s^{-1}), γ is the collision shape factor, χ is the dynamic shape factor, V is the particle speed (m s^{-1}), D is the particle diffusion coefficient (m^2 s^{-1}), ℓ is the apparent mean free path of the particle (m), and g_i or g_j is the distance between the real surface of the i^{th} or j^{th} particle and the spherical surface enclosing the actual particle as assumed by Fuchs [27, 29]. C is the Cunningham correction factor for each particle. ε is the collision coefficient, ρ is the mass density of the particle (kg m^{-3}), g is the gravitational constant (m s^{-2}), V_T is the terminal or settling velocity of the particle (m s^{-1}), ρ_g is the gas density (kg m^{-3}), ε_T is the turbulent energy dissipation rate (m^2 s^{-3}), and υ is the kinematic viscosity (m^2 s^{-1}). The total coagulation kernel is calculated using equation (2-10) as the sum of the three coagulation kernels discussed above.

$$\beta_{total} = \beta_{Brownian} + \beta_{gravitational} + \beta_{turbulence} \quad (2\text{-}10)$$

As should be obvious, the three effects act synergistically and the additive assumption is an approximation.

For better statistics, it would be appropriate to consider larger numbers of particles (~10^{10} or more). Due to the limitations of present-day computational power, the maximum number of particles that can be modeled is about 10^6. Hence, in order to get better statistics, a scaling factor (or weight factor) of 10^6 has been used in the coagulation kernel (that is, the coagulation coefficient is multiplied by the scaling factor) in both the DSMC and the sectional techniques for all the simulations.

2.4.1 Test Problems and Results

For the simulation, a sample seven component problem as described in the MAEROS user manual [13] was considered. Here, *n* particles were simulated each with the particle diameters within the range of 0.01 and 20 microns, and for display purposes, the 20 sections (bins) were used which are logarithmically spaced in particle diameter.

The sections and their associated particle diameter ranges used in the simulations are listed in Table 3. It should be noted that this work does not require the use of such sections. Indeed, the simulations are not based upon the use of sections at all. But these sections have been used only for convenience in the presentation of results and their comparison with the corresponding sectional results.

The DSMC simulation used the seven components listed in Table 4 with their densities specified under the standard temperature and pressure (STP) conditions. The

various values used for the simulation parameters are listed in Table 5. All the values are considered at the STP conditions.

The initial particle number distribution and the distribution after 200 seconds (for 1,000 particles considered initially) are shown in figs. 7 and 8 along with their corresponding component mass distributions. The various shades in the component mass distribution are used to identify components 1 through 7. Since, direct sampling algorithm had computational overheads, the Metropolis sampling algorithm was used which increased the initial particle population from 1,000 to 100,000. The initial distribution and the final distribution after 200 seconds, obtained while using the Metropolis algorithm for collision sampling (using 100,000 particles initially), are shown in figs. 9 and 10 for both particle number and component masses. From these results, it was concluded that the Metropolis algorithm is appropriate to use in place of direct sampling algorithm. Extensive details on these results are given in Palaniswaamy and Loyalka [22].

Table 3: Sections and associate particle diameter ranges.

Sections (Bins)	Particle Diameter Range		Sections (Bins)	Particle Diameter Range	
	Min	Max		Min	Max
1	1×10^{-8}	1.46235×10^{-8}	11	4.47214×10^{-7}	6.53983×10^{-7}
2	1.46235×10^{-8}	2.13847×10^{-8}	12	6.53983×10^{-7}	9.56352×10^{-7}
3	2.13847×10^{-8}	3.12719×10^{-8}	13	9.56352×10^{-7}	1.39852×10^{-6}
4	3.12719×10^{-8}	4.57305×10^{-8}	14	1.39852×10^{-6}	2.04513×10^{-6}
5	4.57305×10^{-8}	6.6874×10^{-8}	15	2.04513×10^{-6}	2.9907×10^{-6}
6	6.6874×10^{-8}	9.77933×10^{-8}	16	2.9907×10^{-6}	4.37345×10^{-6}
7	9.77933×10^{-8}	1.43008×10^{-7}	17	4.37345×10^{-6}	6.39551×10^{-6}
8	1.43008×10^{-7}	2.09128×10^{-7}	18	6.39551×10^{-6}	9.35248×10^{-6}
9	2.09128×10^{-7}	3.05818×10^{-7}	19	9.35248×10^{-6}	0.0000136766
10	3.05818×10^{-7}	4.47214×10^{-7}	20	0.0000136766	0.00002

Table 4: Components and their densities at STP.*

Component	Symbol	Density (kg m^{-3})
Lead	Pb	11,340
Lead Sulphide	PbS	7,600
Lead Oxide	PbO	9,350
Uranium Oxide	UO_2	10,970
Uranium tri-oxide	UO_3	7,300
Sodium Oxide	NaO_2	2,200
Di-sodium Oxide	Na_2O	2,270

* Source: Information on the elements in the periodic table - available at www.webelements.com

Table 5: Simulation parameters and their corresponding values. [13]

Parameter	Symbol	Value	Units
Temperature	T	300	K
Mean free path of air	λ	0.0660	μm
Air viscosity	η	1.81×10^{-5}	kg m^{-1} s^{-1}
Dynamic shape factor	χ	1	Dimensionless
Agglomeration shape factor	γ	1	Dimensionless
Gravitational constant	g	9.81	m s^{-2}
Turbulent energy dissipation rate	ε_T	1	m^2 s^{-3}
Density of air	ρ_g	1.29	kg m^{-3}
Kinematic viscosity of air	υ	1.4031	m^2 s^{-1}

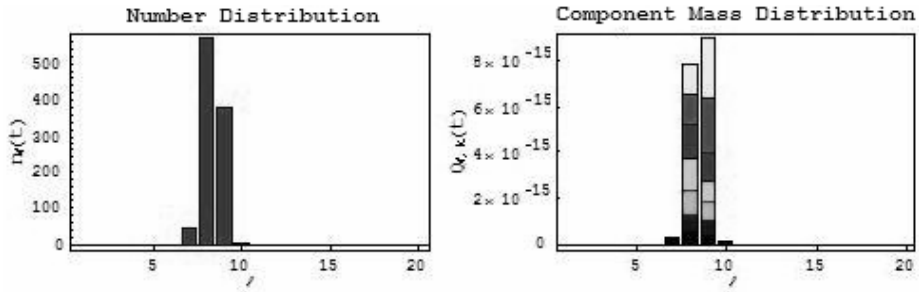

Figure 7: Particle number distribution (left) and component mass distribution (right) for a seven component, complete coagulation kernel – Initial distribution.

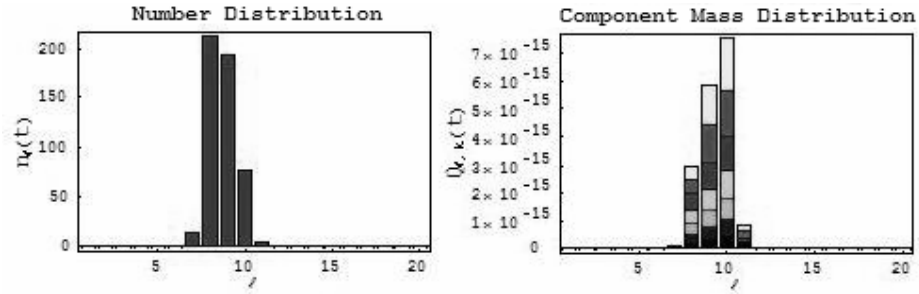

Figure 8: DSMC particle number distribution (left) and component mass distribution (right) for a seven component, complete coagulation kernel – Distribution after 500 collisions.

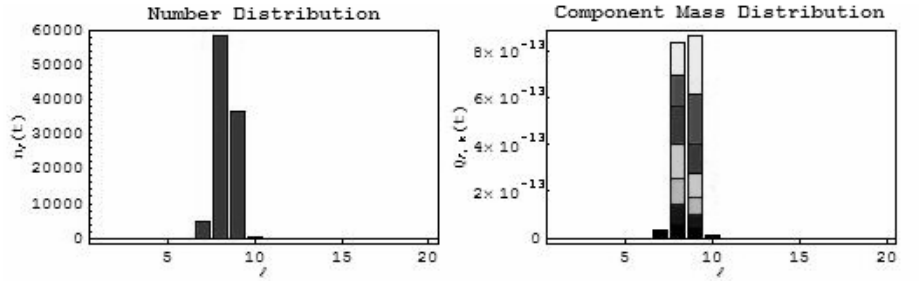

Figure 9: Particle number distribution (left) and component mass distribution (right) for a seven component, complete coagulation kernel – Initial distribution.

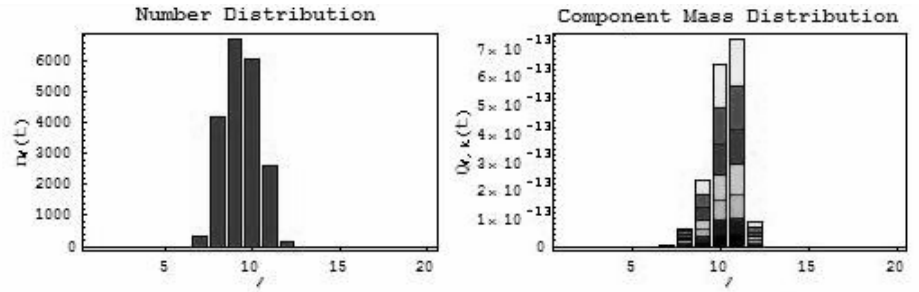

Figure 10: DSMC particle number distribution (left) and component mass distribution (right) for a seven component, complete coagulation kernel – Distribution after 80,000 collisions.

3. COLLISION SAMPLING ALGORITHMS

Collision sampling plays an important role in the simulation of aerosol coagulation. Also, the conventional way of sampling particles for collision – the Direct sampling algorithm, is time and space inefficient. Hence, it becomes necessary to explore other efficient ways of sampling particles for collision. There are actually several collision sampling algorithms in use. In this chapter, four collision sampling algorithms – Direct sampling, the Metropolis sampling [24], the No Time Counter (NTC) method [23] and modified direct sampling algorithms are explored. Since only the Metropolis algorithm was explored in the previous work, and since, other sampling algorithms were not studied, we researched on the efficiencies of four different sampling algorithms. All the four sampling algorithms are described in this chapter and the several test problems simulated are presented along with their results and discussions.

3.1 Direct Sampling Algorithm

The direct sampling algorithm uses an N × N collisional matrix (N being the total number of particles in the entire population), which gives the probabilities of coagulation occurring between the particles in the population (all combinations considered). This matrix has to be calculated and updated frequently after every collision, which is computationally challenging owing to the limited resources available.

The criterion for sampling a pair of particles selected at random for collision is based on an acceptance rejection technique which can be explained as follows. Let u and v be the particles selected at random for collision. Let $\beta(u,v)$ be the coagulation coefficient for particles, u and v. Let β_{min} and β_{max} be the minimum and maximum coagulation coefficients obtained from the collisional matrix. The criterion for sampling can be mathematically expressed as:

$$Random\ [\beta_{min}, \beta_{max}] \leq \beta(u,v) \tag{3-1}$$

where *Random* [a, b] implies a random number distributed uniformly between a and b. We will be using this nomenclature further in this work. β_{min} and β_{max} describe the limits of the distribution, and $\beta(u,v)$ is compared against a random value chosen from this distribution using an acceptance rejection criterion, (3-1).

The primary calculation which consumes a long time is the determination of β_{min} and β_{max}. This requires the pre-computation of the entire collisional matrix and its continual updating, which increases the computation time to an order of N^2.

3.2 Metropolis Sampling Algorithm

3.2.1 Markov Chains

The Markov chain is represented as a sequence of random variables chosen from a state space such that the distribution for the current variable depends only on the immediate past [24, 34, 35]. Thus, for a distribution, *P(x)*:

$$P(x_{t+1} \mid x_1, x_2, ..., x_t) = P(x_{t+1} \mid x_t) \tag{3-2}$$

$P(x_{t+1}|x_t)$ is termed as the transition distribution or the stationary distribution. An example of the Markov chain is the Metropolis algorithm. Unlike sampling based on the entire population, the Metropolis algorithm is based on the current and previous samples (the Markov property) such that the average distribution of samples is similar to that sampled from and based on the entire population.

3.2.2 Metropolis Sampling Algorithm

The Metropolis algorithm, formulated by Metropolis et al [24], is based on an acceptance rejection technique for sampling distributions. It is an example of a Markov chain generally used for large scale calculations and simulations in Physics and Statistics. Basically, the Metropolis algorithm is used to sample from a distribution, π when the distribution itself cannot be computed. Hence, a Markov chain is built with π as the stationary (transition) distribution and the initial sample, $\pi(1)$ chosen at random. Now, the next sample in the chain is proposed as $\pi(2)$. The Metropolis ratio, $m(2,1)$ is then calculated as $\pi(2) / \pi(1)$. If the ratio $m(2,1)$ is greater than a random value, then the sample $\pi(2)$ is termed to be accepted, else, it is rejected and another set of samples are chosen for $\pi(2)$. If the sample is accepted, then the procedure is repeated for the next sample, $\pi(3)$ and so on.

We apply this principle to our sampling problem with the initial coagulation coefficient as a randomly chosen value, $\beta(u', v')$ where u' and v' refer to the two particles sampled for collision. Let u and v be the particles sampled for the current

collision with the coagulation coefficient as $\beta(u, v)$. Now, the criteria for sampling can be mathematically expressed as follows [34, 35]:

$$Random\ [0,1] \leq \frac{\beta(u,v)}{\beta(u',v')} \tag{3-3}$$

The same steps are repeated for another new pair of particles, u and v randomly chosen for collision.

This technique does not require any collisional matrix to be calculated, stored and / or updated continually. The use of the Metropolis algorithm avoids the need to pre-compute and update the collisional matrix after every collision. Therefore, it reduces the computational overheads in programming thereby reducing the computation time to a significant extent, an order of N.

3.3 No Time Counter (NTC) Method

The NTC method, introduced by Bird, was considered to be very effective for rarefied gas dynamics [23]. The NTC method is different from the previously explained direct and the Metropolis sampling algorithms in that, it calculates the number of collisions over a time interval while the earlier methods update the collision times after every collision. The NTC method determines the number of collisions to occur during the interval prior to starting the collision process, thereby avoiding the calculation of collision times after every collision. The number of collisions, N_c in a time interval, Δt is calculated using the formula [23]:

$$N_c = \frac{1}{2} N^2 \beta_{max} \Delta t \tag{3-4}$$

where N refers to the number of particles, and β_{max} refers to the maximum possible coagulation coefficient to be assumed initially. For the number of collisions or collision pairs calculated as N_c, the individual collision pairs are chosen based on an acceptance rejection technique. The two particles, u and v selected at random for collision will be accepted if they satisfy the criterion [23]:

$$Random\ [0,1] \leq \frac{\beta(u,v)}{\beta_{max}} \tag{3-5}$$

During the interval, if the $\beta(u, v)$ for any collision pair exceeds the β_{max}, the $\beta(u, v)$ value is preserved for calculating the number of collisions, N_c for the next interval and hence use the value for the collision sample acceptance rejection criterion. Assuming β_{max}, eliminates the need to pre-compute and periodically update the collisional matrix and also reduces the computation time significantly to the order of N, the number of particles in the population. But determining the number of collisions based on the assumption, β_{max} may not be appropriate for all kinds of problems.

3.4 Modified Direct Sampling Algorithm

Following the Metropolis and the NTC sampling algorithms, we proposed the modified direct sampling algorithm, which, as the name suggests, is a modified version of the direct sampling algorithm, where we assume β_{min} and β_{max}, and continue with the collisional sampling algorithm based on an acceptance rejection technique similar to the one used in the direct sampling algorithm – equation (3-1). This eliminates the use of a collisional matrix and thus helps reduce the computation time significantly from the order of N^2 to an order of N, the number of particles in the population.

Table 6: Summary of collision sampling algorithms.

Technique	**Acceptance Criteria**	**Assumptions**	**Computation Time**
Direct	$Random\ [\beta_{min}, \beta_{max}] \le \beta(u,v)$	-	Order of N^2
Metropolis	$Random\ [0,1] \le \frac{\beta(u,v)}{\beta(u',v')}$	-	Order of N
No Time Counter	$Random\ [0,1] \le \frac{\beta(u,v)}{\beta_{max}}$	β_{max}	Order of N
Modified Direct	$Random\ [\beta_{min}, \beta_{max}] \le \beta(u,v)$	β_{min} and β_{max}	Order of N

Table 6 summarizes the various sampling algorithms that have been explored for a DSMC multi-component aerosol dynamics problem.

3.5 Test Problems

We have verified the correctness of all the three algorithms against the direct sampling algorithm by comparing the sampling distributions of the various algorithms. Also, we have simulated the coagulation process for a DSMC multi-component aerosol dynamics problem using all the four sampling algorithms and compared their results for a variety of test problems. The components used for the simulations are listed in Table 4 (chapter 2) with their densities specified under standard conditions of temperature and pressure. The test problems simulated are listed below.

Test Problem I: Seven component problem using all four sampling algorithms. We use a small initial population (1,000 particles) as the direct sampling technique is time consuming - an order of N^2, and hence, cannot handle a larger population.

Test Problem II: Seven component problem similar to problem set I using modified direct, the Metropolis and the NTC sampling algorithms for a larger population (80,000 particles).

Test Problem III: Seven component problem similar to the problem defined in the MAEROS user manual [13] using modified direct, the Metropolis and the NTC sampling algorithms for a larger population (~70,000 particles).

Table 7: Summary of the test problems.

Test problem	Sampling algorithms used			
	Direct	Metropolis	NTC	Modified direct
I	✓	✓	✓	✓
II	×	✓	✓	✓
III	×	✓	✓	✓

The test problems and the different sampling algorithms used are summarized in table 7.

Test problems I and II have similar initial conditions, except for the initial number of particles simulated, and are explained as follows. We have considered 1,000 and 80,000 particles for the two test problems, respectively, in a volume of 1 m^3 with the particle diameters ranging from 0.01 to 20 microns, having 20 sections logarithmically spaced in particle diameter. The initial mass concentration for all the particles is set to be in a logarithmic distribution.

Test problem III is as described in the MAEROS user manual [13] which considers *n* particles in a volume of 1 m^3 with the particle diameters within the range of 0.01 and 20 microns, having 20 sections logarithmically spaced in particle diameter. Though it is a seven component problem, all the particles initially have only the first component, unlike test problems I and II. The total mass concentration of the particles in section *I* is given by equation (3-6) as:

$$M_I = 10^{-6} e^{-(8(I-1)+1)/4} \quad kg\ m^{-3} \tag{3-6}$$

Particles are generated randomly with a diameter within the range specified by the section limits such that their total mass doesn't exceed the total mass concentration specified for the section. Thus, the equation relating the mass and volume of the particles in every section *I* is given by equation (3-7) as:

$$\sum_{p=1}^{n_I} \left(\frac{\pi}{6} D_{p,I}^3 \right) \rho_1 = M_I \tag{3-7}$$

where n_I is the total number of particles in section I, $D_{p,I}$ is the diameter of the p^{th} particle in section I, ρ_I is the density of component 1, as only component 1 is assumed to be present initially and M_I is the total mass concentration of particles in section I.

Since there is a limitation on the computation time and memory usage for the DSMC computations, we have assumed the total mass concentration to be smaller than that specified in equation (3-6), as $1.0 \times 10^{-10} \times M_I$ which resulted in ~70,000 initial numbers of particles. The initial particle number and component mass distributions for the test problems, I, II and III, are shown in fig. 11. The different shades in the component mass distributions represent the seven different components used for the simulation.

Particles in the current work are generated randomly. We have used Mathematica 5.0, which has a built in random number generator. This generator, and the algorithm it is based upon, have been tested extensively, and is believed to repeat only after 10^{400} calls [36]. Thus, our calculations are presumably free of any bias that might arise from pseudo-random number generation not being truly random.

Figure 11: Initial distributions for test problems I – III.

Test Problem	Initial Number Distribution	Initial Component Mass Distribution
I	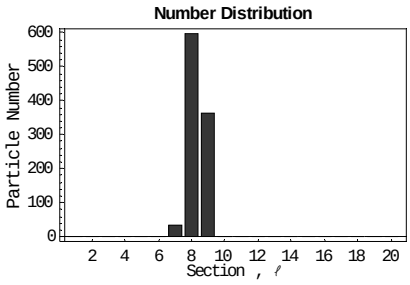	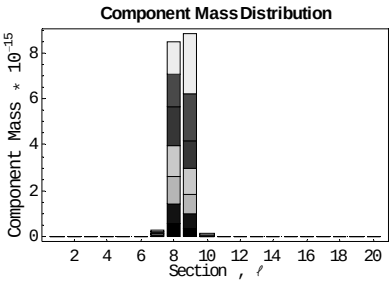
II	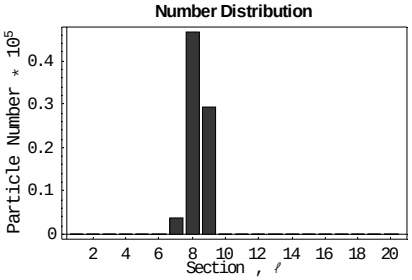	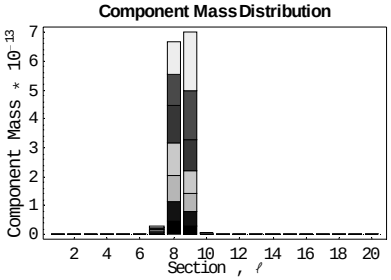
III	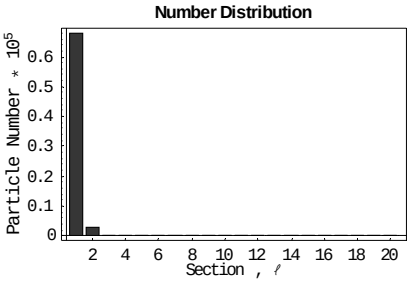	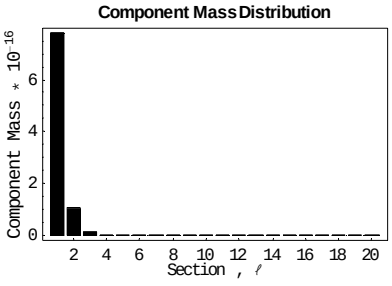

3.6 Results and Discussion

In order to show the appropriateness of the sampling algorithms, the distributions of the collisional sampling algorithms were verified against the distribution obtained using the direct sampling method. For this purpose, we generated the distribution of coagulation coefficients of particles sampled for collision from a population of 1,000 particles experiencing ~985 collisions. The distributions obtained have been plotted in a single plot as shown in fig. 12. The distribution obtained while using the four sampling techniques looks similar, which supports the use of the Metropolis, the NTC and the modified direct sampling algorithms in place of the direct sampling algorithm.

The results obtained for test problem I are shown in fig. 13. The different shades shown in the component distributions indicate components, 1 through 7. A comparison on the distributions obtained using different sampling algorithms as given in fig. 13, shows that the results obtained using both the Metropolis and modified direct sampling algorithms follows those obtained using the direct sampling algorithm. But, the results obtained using the NTC method differs significantly from those obtained using the direct sampling algorithm. This difference is due to the β_{max} assumed for the simulation.

The results obtained for test problem II are shown in fig. 14. A comparison on the particle number and component mass distributions obtained for the algorithms, shows that the results obtained using both the Metropolis and modified direct sampling algorithms are similar while those obtained using the NTC method differ significantly owing to the assumption made for β_{max}.

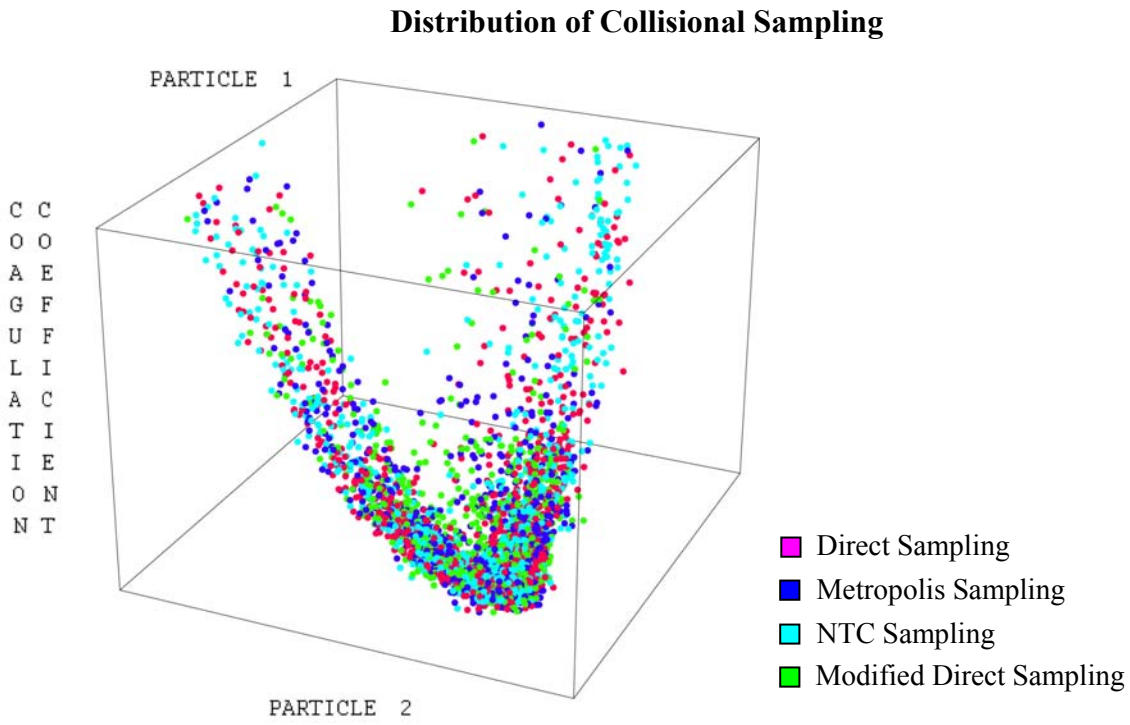

Figure 12: Sampling Distribution – A comparison of the sampling techniques.

Figure 13: Results obtained for Test Problem I after ~900 collisions.

Sampling Algorithms	Number Distribution	Component Mass Distribution
Direct	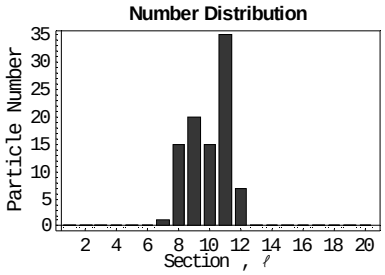	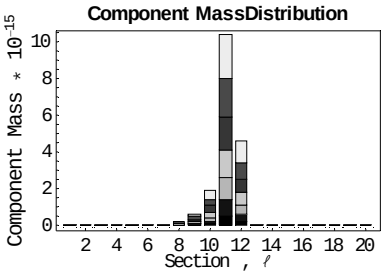
Metropolis	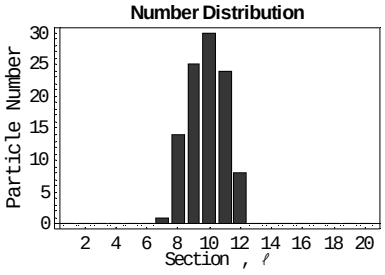	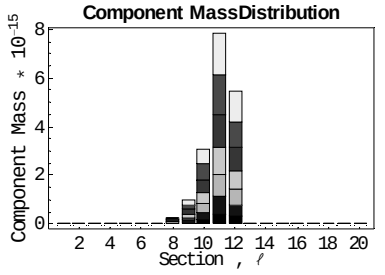
NTC	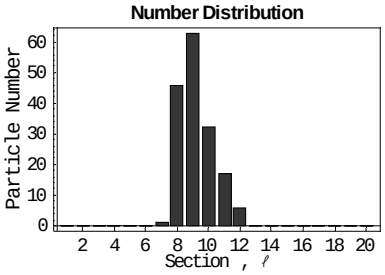	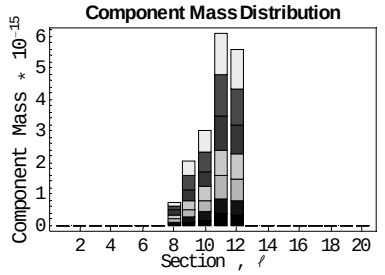
Modified Direct	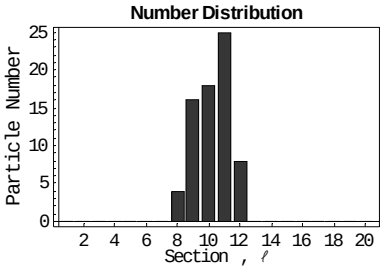	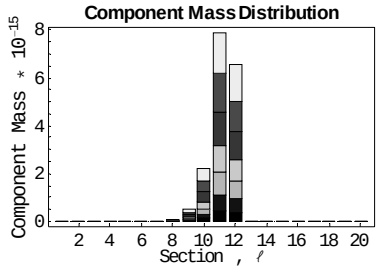

Figure 14: Results obtained for Test Problem II after ~200 seconds.

Sampling Algorithms	Number Distribution	Component Mass Distribution
Metropolis	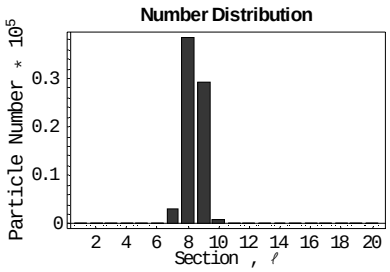	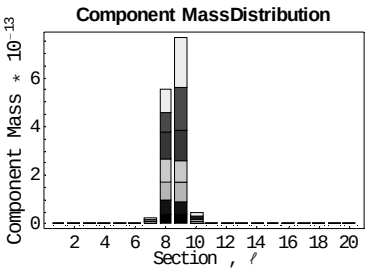
NTC	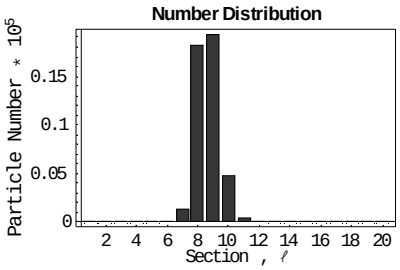	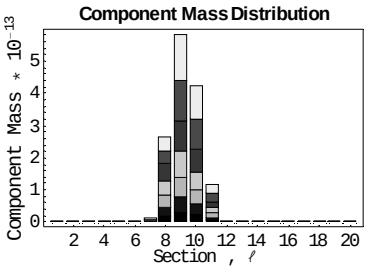
Modified Direct	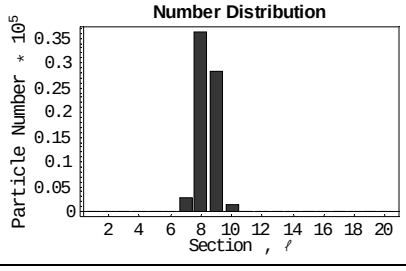	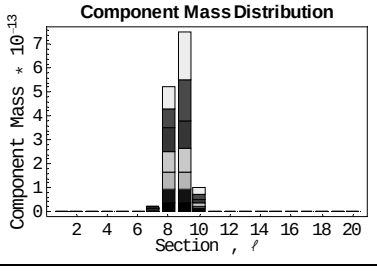

Figure 15: Results obtained for Test Problem III after ~200 seconds.

Sampling Algorithms	Number Distribution	Component Mass Distribution
Metropolis	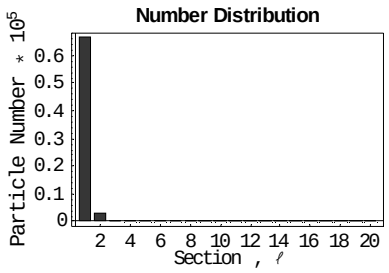	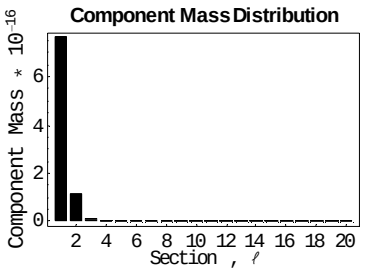
NTC	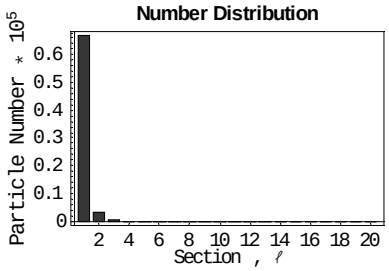	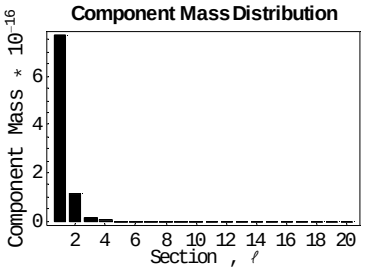
Modified Direct	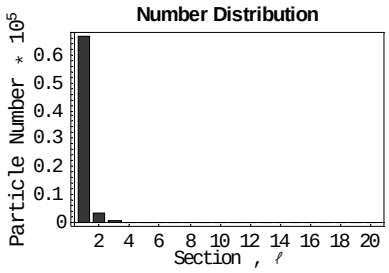	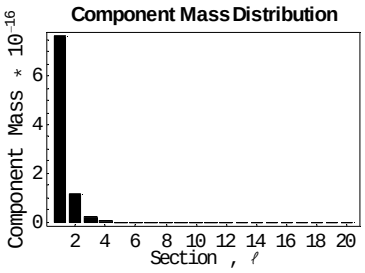

We also compared the results of test problem III using the Metropolis, the NTC and modified direct sampling algorithms. The results of test problem III are shown in fig. 15. The particle number and component mass distributions obtained using all the sampling techniques for test problem III look similar. Though the NTC method gave significantly different results for the previous test problems, it gave agreeable results for test problem III which reassures that the assumption made for β_{max} in the NTC method may not be appropriate for all kinds of problems.

Additionally, test problem III was simulated with the initial mass concentration of $5.0 \times 10^{-10} \times M_I$ which accounted for ~350,000 initial numbers of particles. A plot of the number of particles vs. time for this test problem is shown in fig. 16 which compares the Metropolis, the NTC and modified direct sampling algorithms. Figure 16 shows clearly that the Metropolis algorithm gives better results than the NTC method when compared against the modified direct sampling algorithm. Also, the computation time for the Metropolis sampling algorithm was much less, ~90 seconds, in comparison to the computation times for the NTC and the modified direct sampling algorithms, which were 562 seconds, and 1562 seconds, respectively.

From fig. 16, we conclude that the Metropolis sampling technique provides better results than the NTC method and also, that the Metropolis algorithm works faster than the NTC and modified direct sampling algorithms.

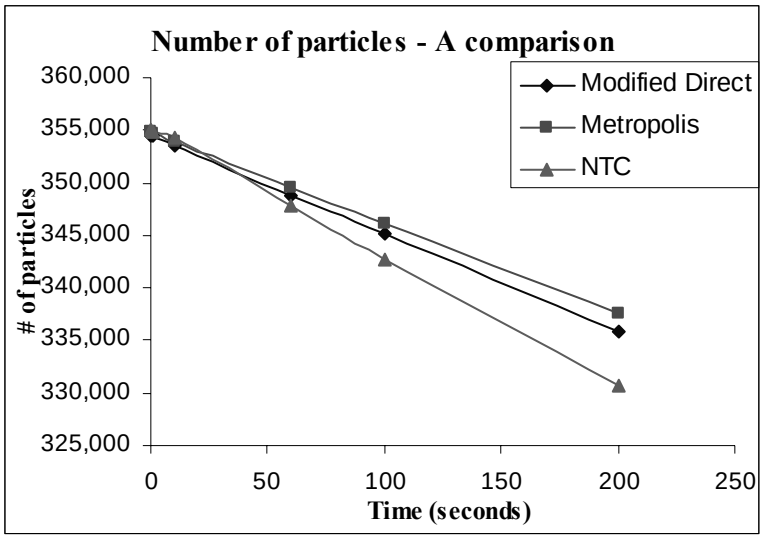

Figure 16: Sampling Algorithms – A comparison.

4. AEROSOL DEPOSITION AND SOURCE REINFORCEMENT

4.1 Aerosol Deposition

Aerosols span a wide range of sizes, from a few nanometers to 100 microns. The larger particles settle more easily due to gravity while the smaller particles diffuse readily and undergo deposition by convection-diffusion. These processes of gravitational settling and convection-diffusion facilitate removal of particles from the entire population simulated and such a process is termed '*deposition*' [16]. Deposition of particles can also be due to thermophoresis which is defined as the process by which particles in a temperature gradient move from a higher temperature region towards a lower temperature region [37, 38]. In this chapter, the effects of gravity and convection-diffusion on deposition have been explained. Gravitational settling, $R_{gravity}$ (s^{-1}) is calculated using equation (4-1) as [13, 39, 40]:

$$R_{gravity} = -\frac{A_{floor}\ V_T}{V_{chamber}} \tag{4-1}$$

where A_{floor} is the floor area (m^2), and $V_{chamber}$ is the chamber volume (m^3). V_T is the particle settling velocity ($m\ s^{-1}$) and is defined as:

$$V_T = \frac{\rho_p\ g\ d^2\ C}{18\ \eta\ \chi} \tag{4-2}$$

where ρ_p is the particle density (kg m^{-3}), g is the acceleration due to gravity (m s^{-2}), d is the particle diameter (m), η is the gas viscosity (kg m^{-1} s^{-1}), χ is the dynamic shape factor (dimensionless), and C is the Cunningham factor (dimensionless). The diffusional deposition is calculated as shown in equation (4-3) [13]:

$$R_{diffusional} = -\frac{D}{\Delta}\left(\frac{A_{wall}}{V_{chamber}} + \frac{A_{floor}}{V_{chamber}} + \frac{A_{ceiling}}{V_{chamber}}\right) \tag{4-3}$$

where A_{wall} is the area of the wall (m^2), $A_{ceiling}$ is the area of the ceiling (m^2), Δ is the diffusion boundary layer thickness (m), and D is the particle diffusivity or diffusion coefficient (m^2 s^{-1}). $R_{gravity}$ and $R_{diffusional}$ represent the rates of particle deposition (s^{-1}) occurring due to the effects of gravity and convection-diffusion, respectively. The total deposition rate is given by the sum of $R_{gravity}$ and $R_{diffusional}$. Computation of these rates, as applied to nuclear aerosol codes, has been discussed in some detail by Fernandes and Loyalka [38, 39].

4.2 Aerosol Source Reinforcement

Aerosols are released from the primary and secondary coolant systems and into the containment at specific source rates during nuclear reactor accidents. This phenomenon of adding aerosols to the volume of study in the form of new particles is called Source Reinforcement [16, 40]. These source particles will coagulate amongst themselves as well as with pre-existing aerosols, and affect the overall aerosol deposition and evolution.

4.3 DSMC Implementation

The DSMC simulation is implemented in the same way as described earlier in chapter 3 – test problem III, where n particles are considered in a volume of 1 m^3 with particle diameters from 0.01 to 20 microns divided into 20 sections logarithmically spaced in particle diameter. The sections (bins) and their associated particle diameter ranges are listed in Table 1. A multi-component, aerosol dynamics problem is considered for this work, where all the particles present initially contain only the first component. The total mass concentration of particles in section I is given by equation (3-6).

Also, after every collision, components 2 through 7 are added to section 1 at a rate specified in the MAEROS user manual [13] as $10^{-9} / I^2$ kg m^{-3} s^{-1} where I refers to the component being added. The source rate is an arbitrary expression. The source thus defined is distributed uniformly as new particles in the entire volume. These new particles are made of components 2 through 7 and do not include component 1 in their composition. So, in summary, it can be said that, for all our test problems, new particles with particle sizes corresponding to section 1 are being generated at a constant rate.

We assume that coagulation, deposition, and source reinforcement occur during a predetermined set of very short time intervals, Δt. As deposition rates are higher than particle coagulation rates, we have considered the deposition of particles to occur first during the time interval, Δt, followed by the coagulation of particles during the same time interval, Δt and finally, we allow source reinforcement to occur for the same time interval, Δt again.

The coagulation, deposition, and source reinforcement processes are integrated in this fashion for all of the test problems and particle compositions. The order of these processes can be deterministically changed depending upon the detailed statement of a particular problem, or can be ordered stochastically. Several test problems have been simulated for different combinations of the coagulation and deposition processes; both in the presence and absence of source reinforcement. The test problems simulated and the simulation results obtained are presented and discussed in greater detail in the following sections. Also, we need to note that significant work has been carried out in this area by Simons [41], Corner and Pendlebury [42], Williams and Loyalka [11], Fernandes and Loyalka [38, 39], and few others.

4.4 Test Problems

4.4.1 DSMC vs. Analytical: A Comparison

We first consider a simple situation in which the number of particles in a volume under consideration is represented as a function of time, $n(t)$. Let us initially assume only deposition occurring at a constant rate represented by λ. The GDE for such a process is:

$$\frac{dn(t)}{dt} = -\lambda\, n(t) \tag{4-4}$$

This is a very simple ordinary differential equation. With the initial condition, $n(0) = n_0$, the solution is given by:

$$n(t) = n_0 e^{-\lambda t} \tag{4-5}$$

When coagulation occurs in addition to the deposition process, then the GDE for the coagulation and deposition processes occurring simultaneously is given by:

$$\frac{dn(t)}{dt} = -\frac{1}{2}\beta n^2(t) - \lambda n(t) \qquad (4\text{-}6)$$

where β is the coagulation rate constant and λ is the deposition rate constant. This ordinary differential equation can be solved for the same initial condition: $n(0) = n_0$ such that,

$$n(t) = e^{-\lambda t}\left[\frac{1}{n_0} + \frac{1}{2}\frac{\beta}{\lambda}\left(1 - e^{-\lambda t}\right)\right]^{-1} \qquad (4\text{-}7)$$

Figure 17 is a plot of the number of particles, $n(t)$, as a function of time, and compares the results obtained from both the DSMC and the above described analytical technique for a single component problem with both coagulation and deposition kernels. The single component in this problem is assumed to be water with ρ = 1,000 kg m^{-3}.

The DSMC and analytical results, when plotted together, trace the same curve as shown in fig. 17, and are indistinguishable. Here, we have used β = 2.4 × 10^{-7} s^{-1} and λ = 0.001 s^{-1} for both the DSMC and analytical techniques. Other, more specific, test problems and simulations, their initial conditions, and the results obtained, are explained further in this chapter.

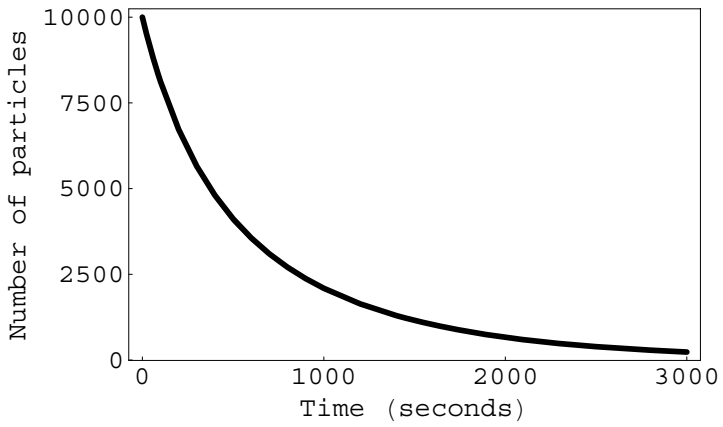

Figure 17: Variation of the number of particles with time. The thin curve represents one realization of the DSMC results. The thick curve represents analytical results ($\beta = 2.4 \times 10^{-7}$ s^{-1} and $\lambda = 0.001$ s^{-1}). As shown, the two curves are indistinguishable.

4.4.2 More Significant Test Problems

We have simulated the following combinations of aerosol processes for several test problems with different particle compositions.

i. Coagulation alone (C)
ii. Deposition alone (D)
iii. Coagulation and deposition (CD)
iv. Source reinforcement alone (S)
v. Coagulation and source reinforcement (CS)
vi. Deposition and source reinforcement (DS)
vii. Coagulation, deposition and source reinforcement (CDS)

The various processes included in each test run and the particle component sets considered for every test run are listed in Table 8. The DSMC results obtained for the set of test runs for a seven-component, aerosol dynamics problem with the same component densities have been compared with the sectional results. The DSMC and the sectional results obtained for these test conditions have been presented in the following section. Since the sectional technique cannot handle different densities, only the DSMC results were obtained for the seven-component and the two-component, aerosol dynamics problems with different component densities.

Table 8. Summary of test problems.

Particle Composition / Processes	Seven-component, Constant Density	Seven-component, Different Density	Two-component, Different Density
C	✓	×	×
D	✓	✓	✓
S	✓	✓	×
CD	✓	✓	✓
CS	×	✓	✓
DS	×	✓	✓
CDS	✓	✓	✓

Table 9. Components and their densities at STP.*

Component	Symbol	Density (kg m^{-3})
Uranium Oxide	UO_2	10,970
Water	H_2O	1,000
Tellurium	Te	6,240
Boron Oxide	B_2O_3	2,550
Cadmium	Cd	8,650
Lead	Pb	11,340
Cesium Iodide	CsI	4,510

* Source: Information on the elements in the periodic table from www.webelements.com

4.4.3 Initial Conditions for the Test Problems

The initial conditions considered are the same for all the test problems and are obtained from the MAEROS user manual [13]. Particle diameters are in the range of 0.01 and 20 μm, and are divided into 20 sections, logarithmically spaced. The seven components and their densities used for seven-component, aerosol dynamics problems with different component densities are given in Table 9. All the values reported correspond to STP conditions.

For the seven-component, same component density test problems, the total mass concentration initially present is obtained from equation (3-6). Since there are limitations on the computation time and memory usage available for the DSMC computations, we have assumed the total mass concentration to be smaller than that specified in equation (3-6); specifically, $1.0 \times 10^{-9} \times M_I$. This accounts for ~805,000 initial particles. Also, we have assumed that the new particles being added to section 1 have a total particle mass of $1.0 \times 10^{-17} / I^2$ kg m^{-3} where I refers to the component being added. The particle diameter of n_I particles being added in each section has been assumed to follow an arithmetic progression. A density of 1,000 kg m^{-3}, representing the density of water, has been assumed for all the seven components. A comparative study of the DSMC and sectional results obtained for several test cases are presented in the following section.

For the seven-component, different component density test problems, the total mass concentration initially present is assumed to be $5.0 \times 10^{-8} \times M_I$ which correspond to ~4 million particles. The source rate being added to section 1 every second is assumed to

have a total particle mass concentration, inclusive of components 2 through 7, of $5.0 \times 10^{-17} / I^2$ kg m^{-3} where I refers to the component being added. The seven components and their densities used for these test runs are given in Table 9. The DSMC results obtained for the test runs listed in Table 8 are presented later in this chapter.

During reactor accidents and/or accidental releases of radioactive materials to the containment, the radioactive elements interact with non-radioactive elements undergoing coagulation and deposition. The two-component, different component density test problem analyzes one such condition specified in Williams and Loyalka [11], where an accident in an LMFBR (Liquid Metal-cooled Fast Breeder Reactor) releases aerosols containing a mixture of non-radioactive sodium oxide and radioactive fuel elements into the containment. It is assumed that the non-radioactive particles are present in the initial aerosol in large numbers. The total mass concentration present initially is assumed to be $1.0 \times 10^{-8} \times M_I$ which correspond to ~3.7×10^6 particles. The source rate being added to section 1 every second is assumed to have a total particle mass concentration, inclusive of components 2 through 7, of $1.0 \times 10^{-17} / I^2$ kg m^{-3} where I refers to the component being added. The DSMC results obtained for the set of test runs listed in Table 8 are presented in the following section. The two components and their densities considered in these test runs are:

Component 1: Sodium Oxide, density: 2,270 kg m^{-3}

Component 2: Uranium Oxide, density: 10,970 kg m^{-3}

Finally, in an effort to study the effect of different component densities, we have simulated the DSMC seven-component test problem for three different cases involving

different component densities in the presence of aerosol processes such as coagulation, deposition, and source reinforcement. The initial conditions for all three cases with different component densities are: an initial mass concentration of $1.0 \times 10^{-9} \times M_I$, consisting of component 1 only, and a source rate being added only to section 1 every second assumed to have a total particle mass concentration, inclusive of components 2 through 7, of $1.0 \times 10^{-19} / I^2$ kg m^{-3} where I refers to the component being added. For these test problems, the initial mass concentrations are considered to be the same and the following three different cases of component densities are considered.

i. Same component density, assuming the density of water – a case similar to that specified in the MAEROS user manual [13].

ii. Different component densities with water present initially, in order to make sure that component 1 is the same as in the problem specified above. Components 2 – 7 are the same as listed in Table 9.

iii. Different component densities with UO_2 present initially and the remaining components as listed in Table 9 – an approximate accident scenario.

Every test run listed in Table 8 is simulated for 200 seconds, and the particle number and component mass distributions are analyzed after 200 seconds. Since there were no particles present in any sections beyond section 7, all of the distributions have been formatted to show only sections 1 through 7.

4.5 Results and Discussions

4.5.1 DSMC vs. Sectional: A comparative study

The initial distribution and the particle number and component mass distributions after 200 seconds for all of the test cases run using the DSMC and the sectional techniques are shown in figs. 18 and 19, respectively. For the initial distribution of $1.0 \times 10^{-9} \times M_I$, the DSMC calculations resulted in ~805,000 initial particles while the sectional calculations had 927,551 initial particles. The difference of ~13% between these numbers is due to the random behavior inherent in the DSMC approach. A comparison of the results from figs. 18 and 19 show that the DSMC results agree well with those of the sectional method.

Though the test problem is for a seven-component aerosol dynamics problem, the initial component mass distributions in figs. 18 and 19 show only component 1 due to the initial problem set up. Components 2 through 7 show up in the distributions only when new particles are added at a constant rate by the source reinforcement process as included in cases S and CDS. The different shades in the component mass distributions for the S and CDS cases in figs. 18 and 19 correspond to components 2 through 7. Using the DSMC technique, 5,058 particles are added every second. Though the mass concentration of particles being added is the same, 5,831 particles were added every second, while using the sectional technique. Again, there is a difference of ~13% between the DSMC and the sectional technique due to the fundamental difference in the DSMC and the sectional approaches.

From figs. 18 and 19, it can be seen that the DSMC and the sectional results agree well with each other except for some subtle differences which are due to the randomness of the DSMC approach and to the differences in the initial distributions. Comparing the initial distributions and the distributions after 200 seconds for case D, it can be seen that ~96.5 % of the particles were deposited within 200 seconds (note that the scale for the graph has been changed). As the particle population decreases, the relevant statistics get poorer. Hence, the distributions in cases D and CD develop significant differences between the DSMC and the sectional results.

Table 10 shows a listing of the number of particles present at different times as calculated using the DSMC and the sectional techniques for a seven-component, same component density, aerosol dynamics problem for the D, CD, and CDS cases. A plot of the data in Table 10 is shown in fig. 20, where it can be seen that the DSMC results agree well with the sectional results. We have assumed that the initial total mass concentration is $1.0 \times 10^{-9} \times M_I$ and also that the new particles being added to section 1 have a total mass concentration, inclusive of components 2 through 7, of $1.0 \times 10^{-17} / I^2$ kg m^{-3} (where I refers to the component being added).

Figure 18: Test results for a same component density problem using the DSMC technique.

Test Cases	Number Distribution	Component Mass Distribution
Initial	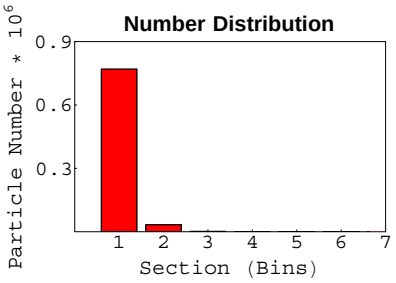	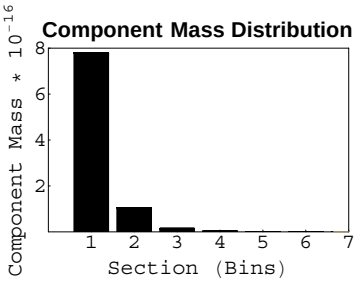
C (200 s)	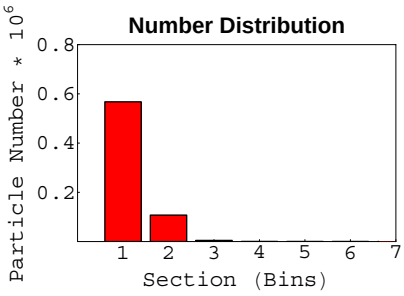	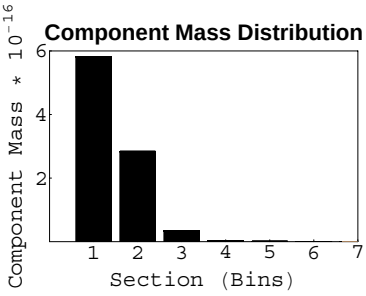
D (200 s)	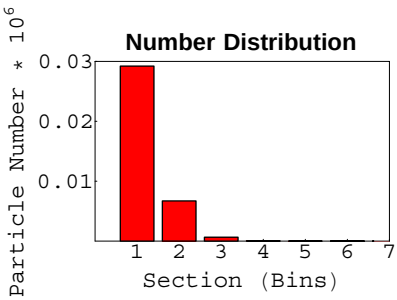	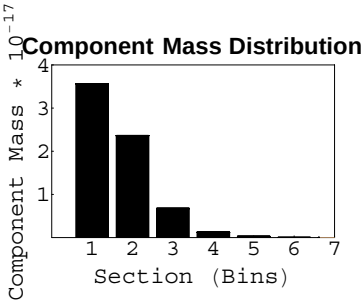
CD (200 s)	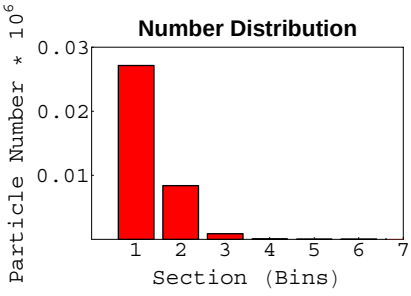	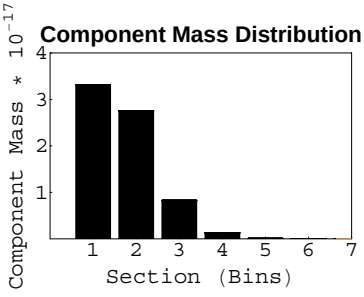

S (200 s)	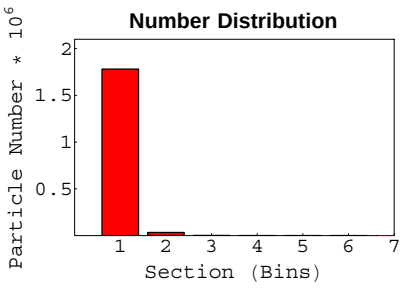 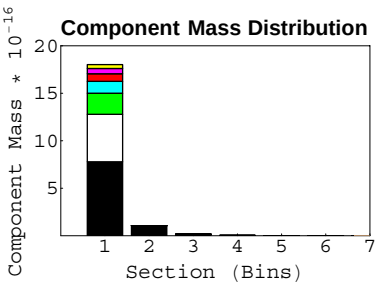
CDS (200 s)	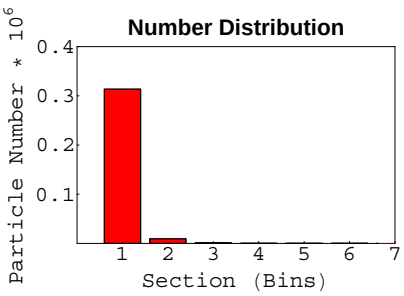 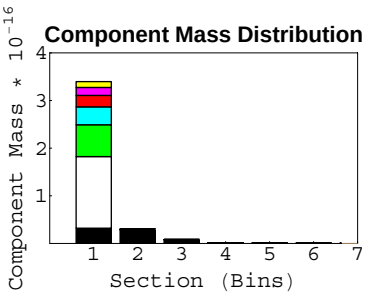

Figure 19: Test results for a same component density problem using sectional technique.

Test Cases	Number Distribution	Component Mass Distribution
Initial	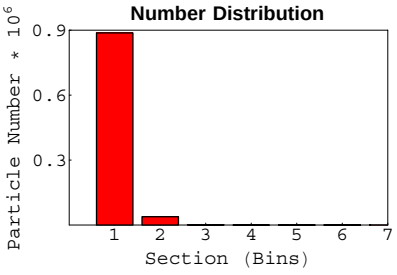	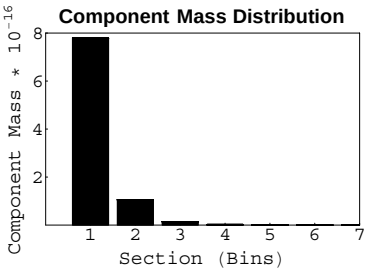
C (200 s)	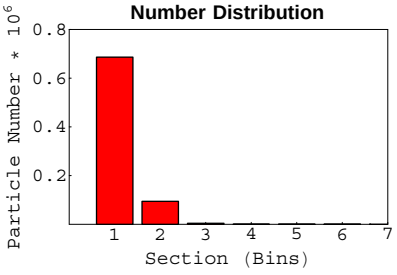	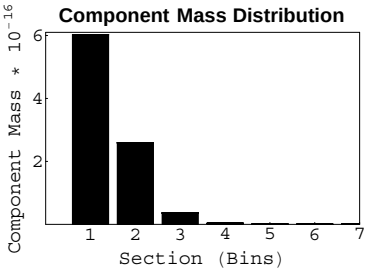

D (200 s)	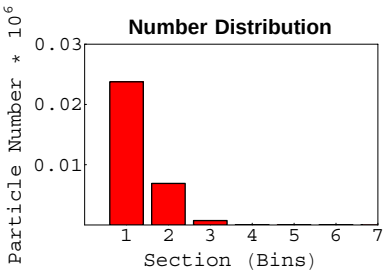	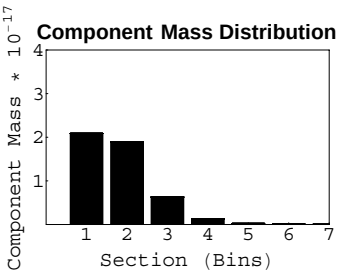
CD (200 s)	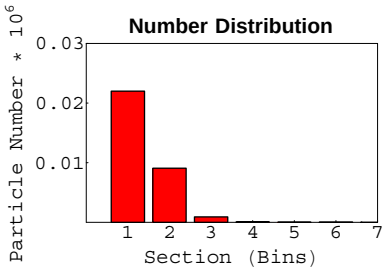	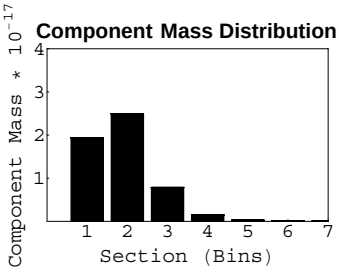
S (200 s)	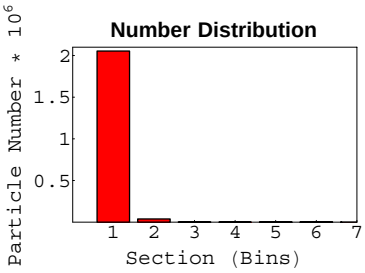	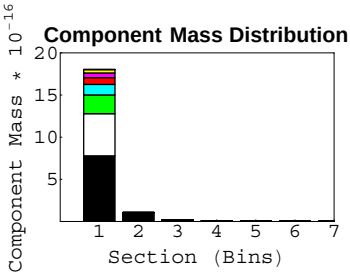
CDS (200 s)	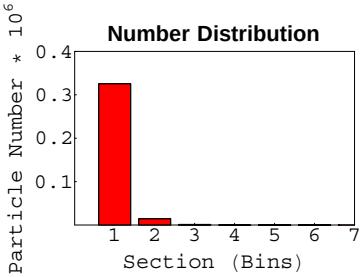	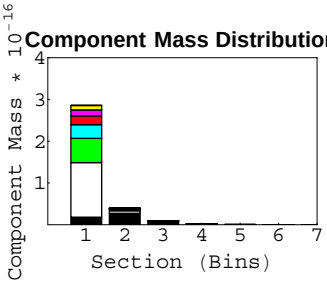

Table 10. Comparison of the DSMC vs. sectional techniques.

Time in seconds	Number of particles in suspension					
	Case D		Case CD		Case CDS	
	DSMC	Sectional	DSMC	Sectional	DSMC	Sectional
0	804,881	927,551	804,451	927,551	804,958	927,551
1	790,998	911,282	789,450	910,473	794,970	916,247
10	677,179	777,362	667,757	771,167	714,921	824,060
60	294,280	323,833	282,258	315,423	471,475	523,911
100	156,194	162,643	149,804	158,743	389,004	422,183
200	35,995	31,438.70	36,589	32,041.70	324,104	341,120
300	10,022	7,337.49	10,708	8,086.54	308,806	325,521
400	3,403	2,231.26	3,786	2,656.50	303,540	321,617
500	1,336	871.27	1,600	1,085.10	302,335	320,319

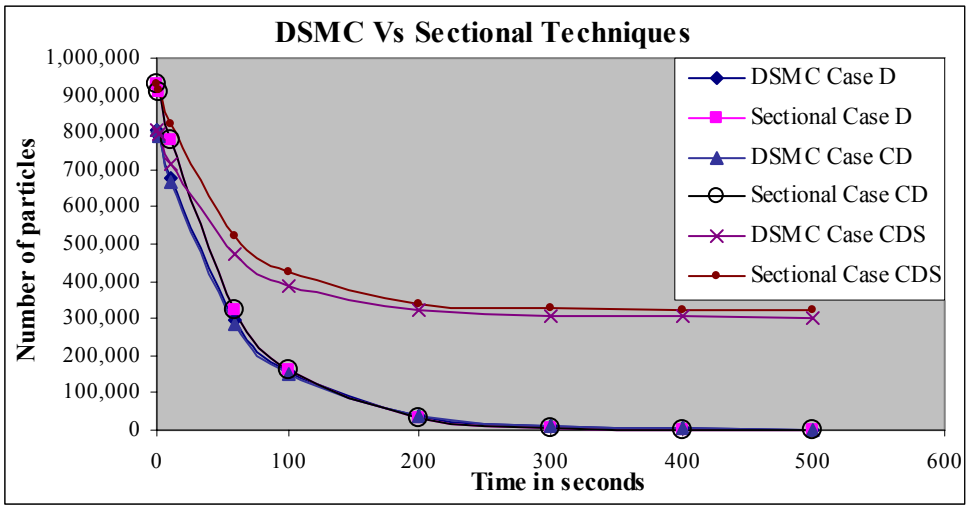

Figure 20: DSMC vs. Sectional - A comparison.

4.5.2 DSMC Seven-Component, Different Component Density Problem

The seven components used for this simulation are listed in Table 9. The initial number of particles for each of the test cases is about 3.7×10^6. The initial total component mass concentration is $5.0 \times 10^{-8} \times M_I$, as specified in the initial conditions. The initial distributions and the particle number and component mass distributions after 200 seconds for all test cases are shown in fig. 21. Here too, the initial component mass distribution shows only component 1 as the problem defines only component 1 to be present initially. For the test cases involving source reinforcement, the source rate added to section 1 every second is assumed to be $5.0 \times 10^{-17} / I^2$ kg m^{-3} (where I refers to the component being added). This corresponds to ~15,000 particles added per second. The different shades in the component mass distribution for cases S, CS, DS and CDS show new particles with components 2 through 7. It can be observed in fig. 21 that particle coagulation does not have a significant effect because particle deposition dominates the loss process. Also, since the source adds only components, 2 through 7 to the volume and not component 1, after few hundred seconds, component 1 will deplete and components, 2 through 7 will become more prominent in the distributions.

Figure 21: Results obtained for a seven-component different component density problem.

Test Cases	Number Distribution	Component Mass Distribution
Initial	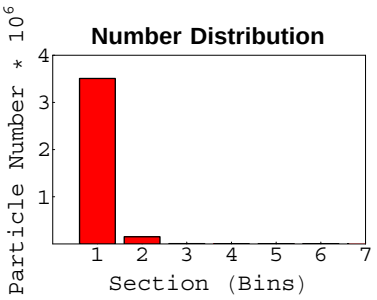	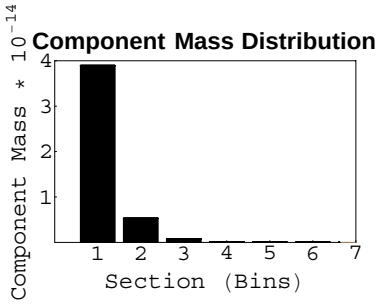
D (200 s)	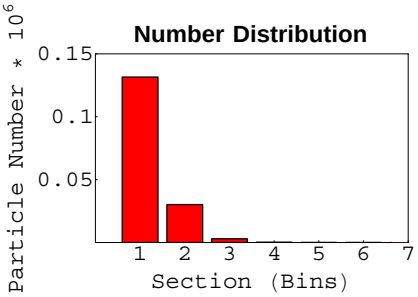	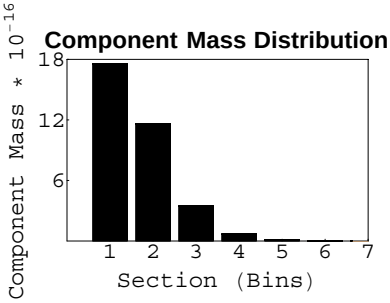
CD (200 s)	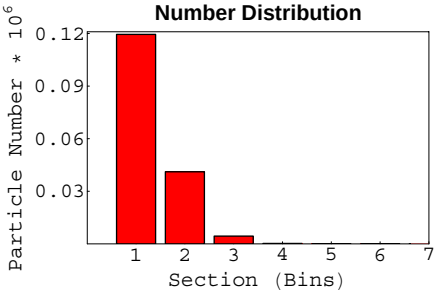	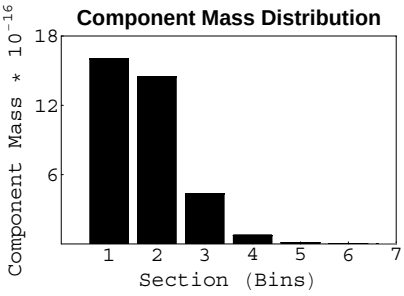
S (200 s)	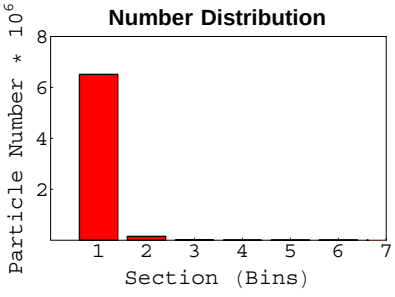	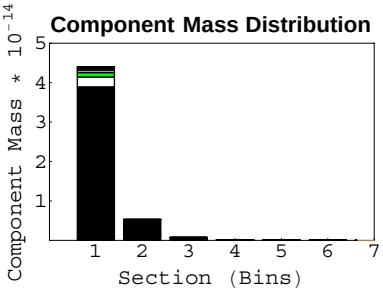

CS (200 s)	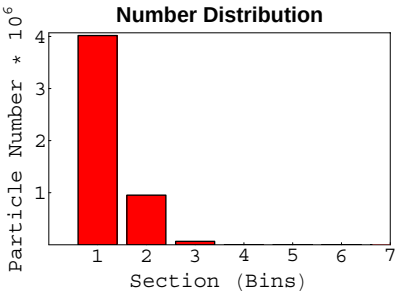	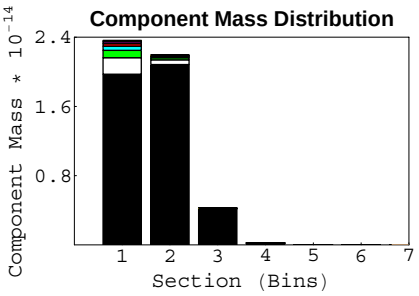
DS (200 s)	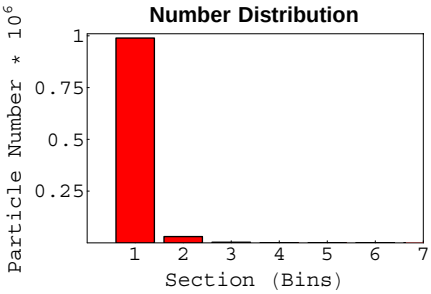	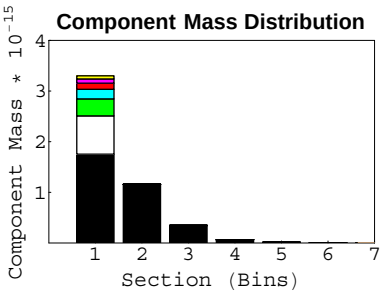
CDS (200 s)	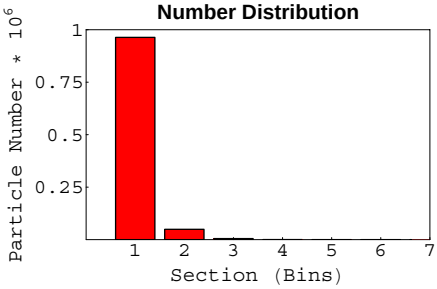	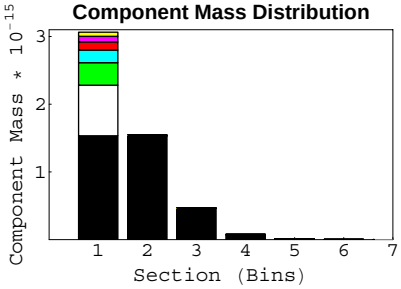

4.5.3 DSMC Two-Component, Different Component Density Problem

Figure 22 shows the DSMC results for the two-component, different component density, aerosol problem which is a simple case that occurs in the reactor containment during an accident. The different shades in the component mass distributions for cases CS, DS and CDS represent components 1 and 2. We have considered the total mass concentration to be $1.0 \times 10^{-8} \times M_I$. This corresponds to an initial number of particles of $\sim 3.7 \times 10^6$. Also, 324 particles were added every second as determined by the source rate, $10^{-17} / I^2$ kg m^{-3} (where I refers to the component being added).

In figs. 21 and 22, it can be observed that the concentration of component 1 decreases rapidly in the first few hundred seconds due to the deposition process being dominant.

Figure 22: Results obtained for a two-component, different component density problem.

Test Cases	Number Distribution	Component Mass Distribution
Initial	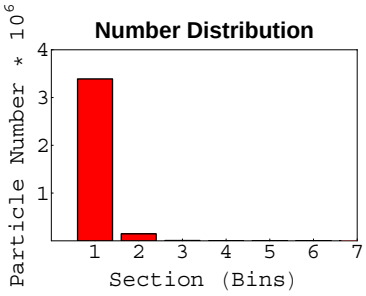	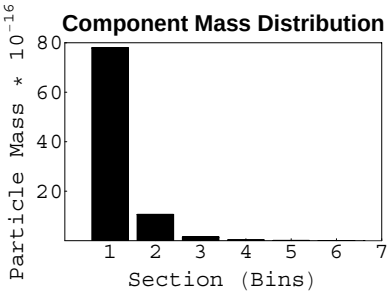
D (200 s)	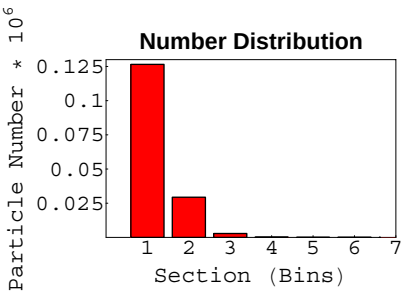	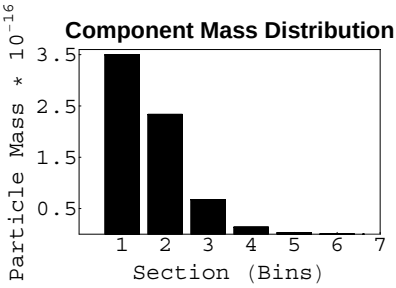
CD (200 s)	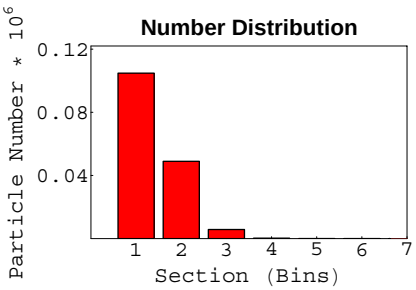	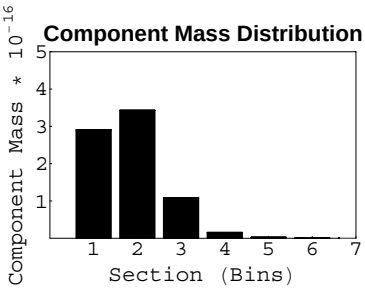
CS (200 s)	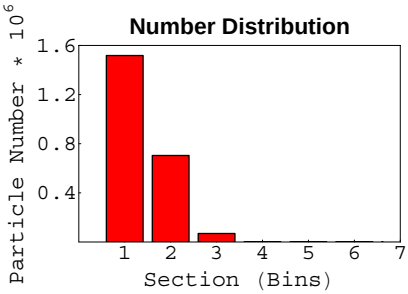	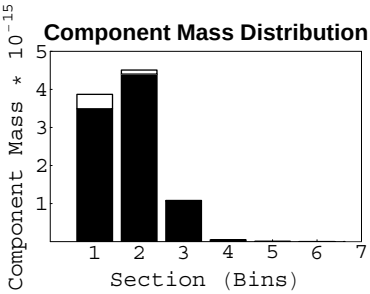

DS (200 s)	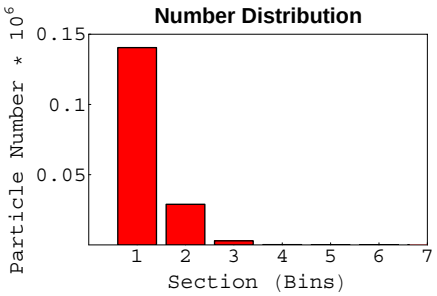	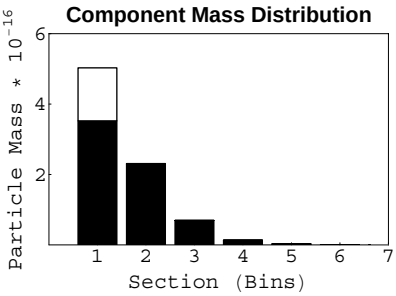
CDS (200 s)	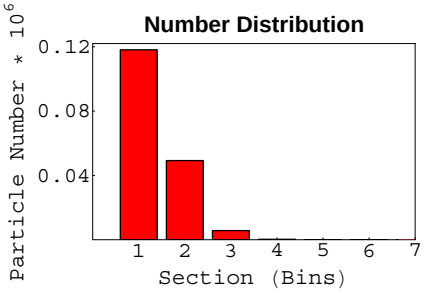	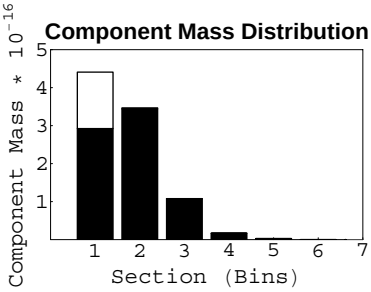

4.5.4 Effect of different component densities

The component mass and particle number distributions obtained for the three different cases of component densities in the presence of aerosol processes such as coagulation, deposition, and source reinforcement at different times have been tabulated in figs. 23 and 24. Though the initial mass concentrations and the source rates were the same for all three cases, the particle numbers were different for case III owing to the differences in the component densities. This difference can be seen in fig. 24 where different scaling is used for case III. From these figures, it can be seen that the results obtained for the problem using the same component density differ significantly from the different component density results. Also, it can be concluded that the assumption made in the MAEROS code [13, 17] regarding the use of a single mean density is not appropriate when simulating multi-component aerosol dynamics problems involving different component densities.

Figure 23: Effect of different component densities on the component mass distribution.

Test Problem I: Same component density	Test Problem II: Different component density	Test Problem III: Different component density
At time, t = 0 seconds. 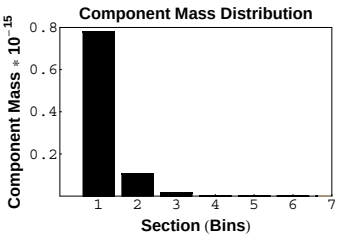	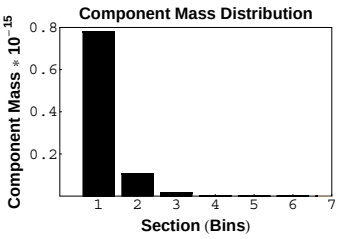	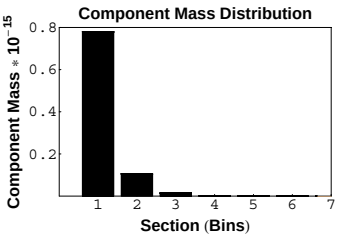
At time, t = 100 seconds. 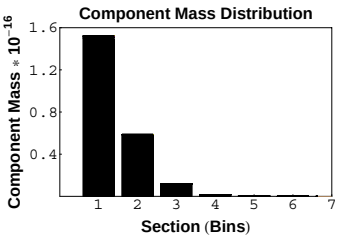	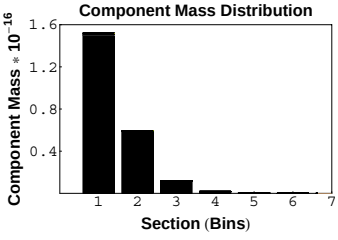	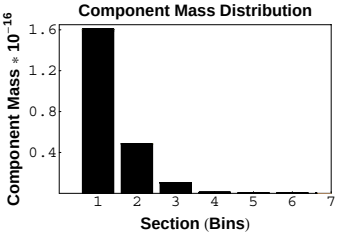
At time, t = 200 seconds. 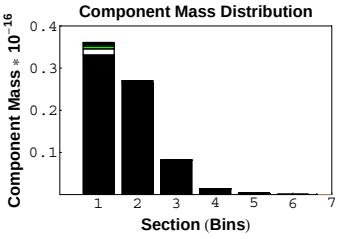	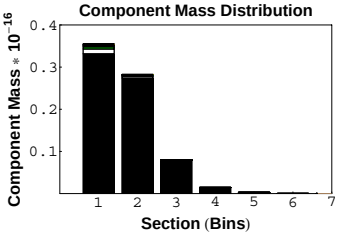	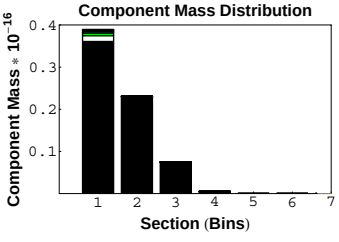
At time, t = 500 seconds. 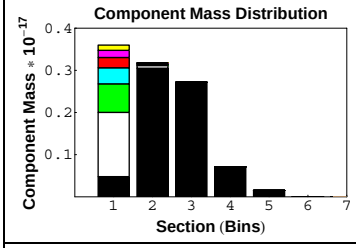	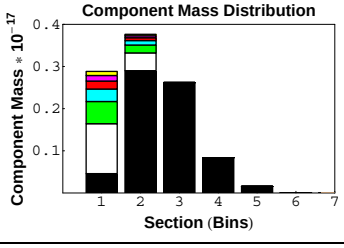	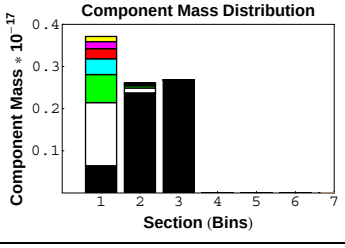
At time, t = 1000 seconds. 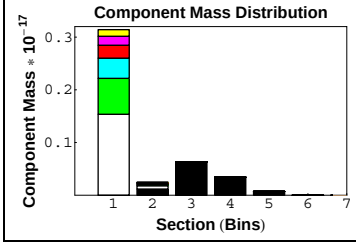	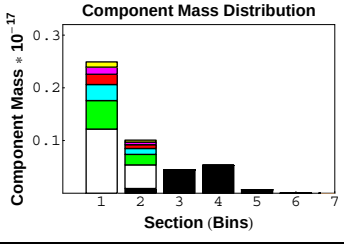	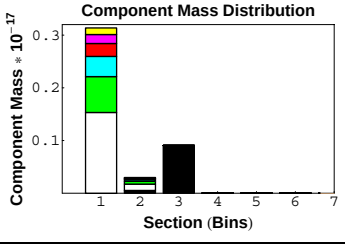

Figure 24: Effect of different component densities on the particle number distribution.

Test Problem I: Same component density	Test Problem II: Different component density	Test Problem III: Different component density
At time, t = 0 seconds. 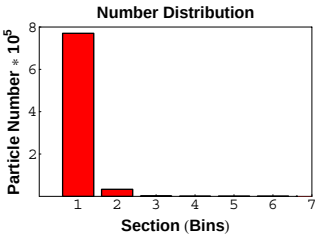	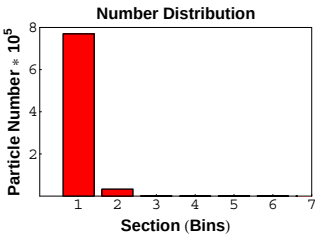	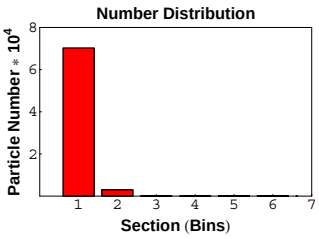
At time, t = 100 seconds. 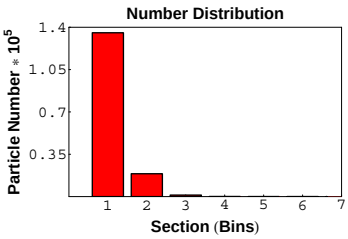	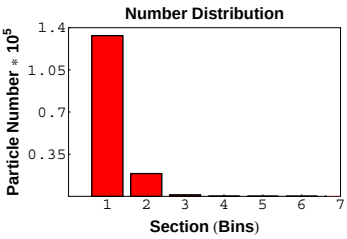	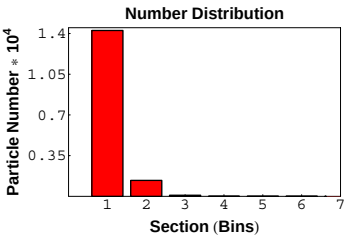
At time, t = 200 seconds. 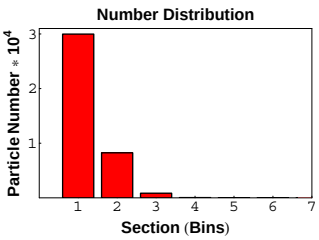	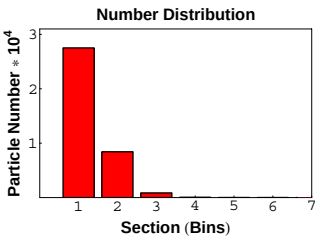	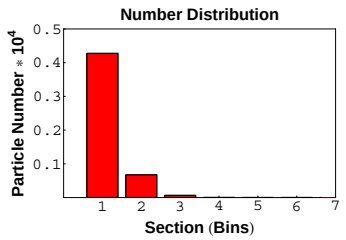
At time, t = 500 seconds. 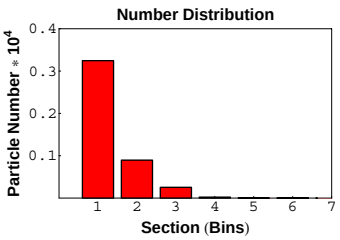	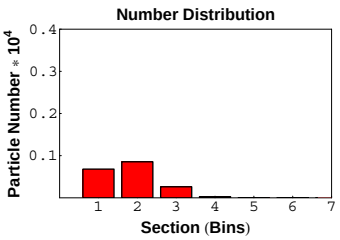	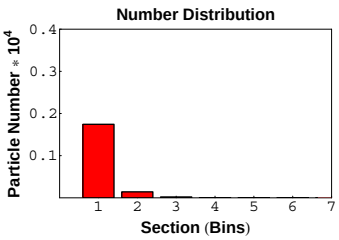
At time, t = 1000 seconds. 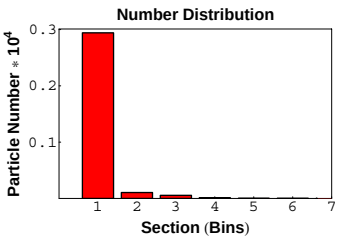	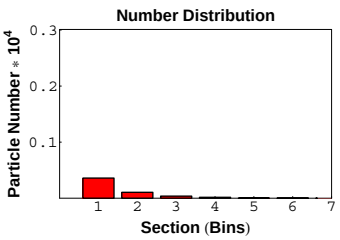	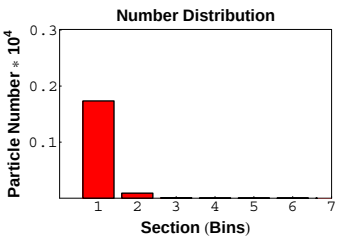

5. AEROSOL CONDENSATION

5.1 Aerosol Condensation

Considering only the condensation process in a spatially homogeneous medium, the aerosol GDE can be expressed as:

$$\frac{\partial}{\partial t} n(\boldsymbol{v},\boldsymbol{m},t) = -\sum_{p=1}^{N} \frac{\partial}{\partial v_p}\left[I_p(\boldsymbol{v},\boldsymbol{m},t)\, n(\boldsymbol{v},\boldsymbol{m},t)\right] \tag{5-1}$$

Considering both coagulation and condensation processes in a spatially homogeneous medium, the aerosol GDE can be expressed as:

$$\begin{aligned}
&\frac{\partial}{\partial t} n(\boldsymbol{v},\boldsymbol{m},t) + \sum_{p=1}^{N} \frac{\partial}{\partial v_p}\left[I_p(\boldsymbol{v},\boldsymbol{m},t)\, n(\boldsymbol{v},\boldsymbol{m},t)\right] \\
&\quad = \frac{1}{2}\int_0^{\infty} d\boldsymbol{u}\int_0^{\infty} d\boldsymbol{w}\int_0^{\infty} d\boldsymbol{q}\int_0^{\infty} d\boldsymbol{s}\; n(\boldsymbol{u},\boldsymbol{q},t)\, n(\boldsymbol{w},\boldsymbol{s},t)\, K(u,q \mid w,s) \\
&\quad \times \prod_{p=1}^{N} \delta(v_p - u_p - w_p)\,\delta(m_p - q_p - s_p) - n(\boldsymbol{v},\boldsymbol{m},t)\int_0^{\infty} d\boldsymbol{u}\int_0^{\infty} d\boldsymbol{q} K(u,q \mid v,m)\, n(\boldsymbol{u},\boldsymbol{q},t)
\end{aligned} \tag{5-2}$$

Assuming only a single component problem, the GDE in equation (5-2) can be simplified to equation (5-3) as:

$$\frac{\partial}{\partial t} n(v,t) + \frac{\partial}{\partial v}\left[I(v,t) n(v,t)\right] = \frac{1}{2}\int_0^{v} K(v,u) n(v-u,t) n(u,t) du - n(v,t)\int_0^{\infty} K(v,u) n(u,t) du \tag{5-3}$$

Note that the particle volumes, v and u, used in equation (5-3) are scalars and the particle number, $n(v,t)$ is independent of the mass of the particle. Various methods of solving integro-differential equations such as this include the finite elements method, the sectional method, the analytical method, and the numerical method among others and have been explained in Williams and Loyalka [11]. Also, there are computer programs (MAEROS [13] in CONTAIN [17], etc.) that solve these equations and simulate the particle number and component mass distributions at various times. Studies have been made in this area by Ramabhadran et al [43], Gelbard and Seinfeld [44], Park and Loyalka [45, 46] and Simons [47].

5.2 Test Problem I: Aerosol Condensation

For the first problem, we consider challenging, single component aerosols undergoing condensation alone. We consider two specific cases for this test problem. Case I considers a constant condensation rate and case II considers the condensate rate, I to be dependent on particle volume, v. The system of equations defining the two test cases with condensation process alone and their corresponding analytical solutions are given in Table 11. Since condensation affects only the particle volume and not the particle number, the system of equations in Table 11 shows only total volume, ϕ as a function of time, t. The initial condition is given as: $\phi(0) = \phi_0$. N_0 is taken as the number of particles present in the system per unit volume, which remains constant with time for this problem as condensation does not change the total number of particles. For initial

conditions, we assume particle diameters to follow a log-normal distribution and the distribution is shown in equation (5-4) as [11, 43]:

$$n(v,0) = \frac{N_0}{v_0} \exp\left[-\frac{v}{v_0} \right] \tag{5-4}$$

where N_0 refers to the initial number of particles per unit volume (m^{-3}) and v_0 is the mean initial volume of the particles present in the distribution (m^3). It needs to be mentioned here that, I and σ_0 have units of $m^3\ s^{-1}$, σ_1 has units of s^{-1}, $\phi(t)$ has units of m^3, and $n(v,t)$ has units of m^{-6}.

Table 11: Condensation problem - Parameters and analytical solutions. [11, 43]

Test Cases	Parameters	System of equations	Analytical Solution
I	$I = \sigma_o$	$\frac{d\phi}{dt} = \sigma_0 N_0$	$\phi(t) = \phi_0 + \sigma_0 N_0 t$
II	$I = \sigma_1 v$	$\frac{d\phi}{dt} = \sigma_1 \phi$	$\phi(t) = \phi_0 \exp\left[\sigma_1 t\right]$

The particle number distribution, $n(v,t)$ as a function of particle size, v and time, t for the two cases is given by equations (5-5) and (5-6), respectively, as [11, 43]:

$$n(v,t) = \begin{cases} \frac{N_0}{v_0} \exp\left[-\frac{(v-\sigma_0 t)}{v_0} \right] & (v-\sigma_0 t) \geq 0 \\ 0 & (v-\sigma_0 t) < 0 \end{cases} \tag{5-5}$$

$$n(v,t) = \frac{N_0}{v_0} \exp\left[-\sigma_1 t\right] \exp\left[-\frac{v}{v_0} \exp\left[-\sigma_1 t\right] \right] \tag{5-6}$$

5.3 Test Problem II: Aerosol Condensation and Coagulation

This problem includes both condensation and coagulation occurring simultaneously. The three test cases considered are given in Table 12. The coagulation and condensation rates are represented by K and I respectively, with the rate constants for coagulation and condensation defined respectively as, K_0, K_1 and σ_0, σ_1 (for test cases, I - III). The system of equations and the corresponding analytical solutions for the three test cases are also given in Table 12. Here again, K, I, K_0 and σ_0 have units of $m^3\ s^{-1}$, K_1 and σ_1 have units of s^{-1}, $\phi(t)$, u and v have units of m^3, $n(v,t)$ has units of m^{-6}, and $N(t)$ and N_0 have units of m^{-3}.

Table 12: Condensation and coagulation - Parameters and analytical solutions. [11, 43]

Test Cases	Parameters	System of equations	Analytical Solution
I	$K = K_0$ $I = \sigma_1 v$	$\frac{dN}{dt} = -\frac{K_0}{2} N^2$ $\frac{d\phi}{dt} = \sigma_1 \phi$	$N(t) = \frac{N_0}{1 + K_0 N_0 t / 2}$ $\phi(t) = \phi_0 \exp[\sigma_1 t]$
II	$K = K_1(u + v)$ $I = \sigma_1 v$	$\frac{dN}{dt} = -K_1 N \phi$ $\frac{d\phi}{dt} = \sigma_1 \phi$	$N(t) = N_0 \exp\left[-\frac{K_1 \phi_0}{\sigma_1} \left(\exp[\sigma_1 t] - 1 \right) \right]$ $\phi(t) = \phi_0 \exp[\sigma_1 t]$
III	$K = K_0$ $I = \sigma_o$	$\frac{dN}{dt} = -\frac{K_0}{2} N^2$ $\frac{d\phi}{dt} = \sigma_0 N$	$N(t) = \frac{N_0}{1 + K_0 N_0 t / 2}$ $\phi(t) = \phi_0 \left[1 + \frac{2\sigma_0}{K_0 \phi_0} \ln\left(\frac{N_0}{N} \right) \right]$

Since coagulation affects the particle population and condensation affects the particle volume, both the particle population, N, and total volume, ϕ, are considered in the system of equations, as functions of time, t, and are shown in Table 12. The initial conditions are specified as: $N(0) = N_0$ and $\phi(0) = \phi_0$. The initial size distribution considered for the particle diameters is given below in equation (5-7) as a log-normal distribution with v_0 as the mean initial volume of the particles in the distribution [11, 43].

$$n(v,0) = \frac{N_0}{v_0} \exp\left[-\frac{v}{v_0} \right] \tag{5-7}$$

Cases I and III consider a constant coagulation rate while case II considers the coagulation rate to be dependent on the volume of the particles sampled for collision, u and v. Also, test cases I and II consider the condensation rate to be dependent on particle volume, v and case III considers a constant condensation rate. The particle number distribution, $n(v,t)$ as a function of particle size, v and time, t for the three cases is given, respectively, by equations, (5-8) – (5-10) as [11, 43]:

$$n(v,t) = \frac{N_0}{v_0}(1-\tau)^2 \exp\left[-\frac{2\Lambda\tau}{(1-\tau)} \right] \exp[-\frac{v}{v_0}(1-\tau) \exp\left[-\frac{2\Lambda\tau}{(1-\tau)} \right]] \tag{5-8}$$

$$n(v,t) = \frac{N_0\omega}{v\sqrt{1-\omega}} \exp\left[-(1-\tau)(2-\omega)\frac{v}{v_0} \right] I_1\left[2(1-\tau)\sqrt{1-\omega}\,\frac{v}{v_0} \right] \quad ;\omega = \exp\left[-\frac{\tau}{\Lambda(1-\tau)} \right] \tag{5-9}$$

$$n(v,\chi) = \frac{N_0 / v_0}{\chi(\chi - 2\Lambda(\chi - 1 - \chi\ln\chi))} \exp\left[-\frac{(v/v_0 - 2\Lambda(\chi-1))}{\chi - 2\Lambda(\chi - 1 - \chi\ln\chi)} \right] \quad \begin{matrix} \chi = 1+\tau \quad and \\ v \geq 2\Lambda v_0(\chi - 1) \end{matrix} \tag{5-10}$$

Table 13: Definitions for symbols, Λ and τ used in equations, (5-8) – (5-10).

Test Cases	Λ	$\tau(t)$
I	$\Lambda = \frac{\sigma_1}{K_0 N_0}$	$\tau = 1 - \frac{2}{2 + K_0 N_0 t}$
II	$\Lambda = \frac{\sigma_1}{K_1 N_0 v_0}$	$\tau = 1 - \exp[\sigma_1 t]$
III	$\Lambda = \frac{\sigma_0}{K_0 N_0 v_0}$	$\tau = K_0 N_0 t / 2$

The definitions of the symbols, Λ and τ used in the above equations for the three cases are shown in Table 13. It has to be noted that both Λ and τ are dimensionless numbers.

The different test problems discussed in this chapter can describe representative cases of practical interest. These sample test problems and their corresponding analytical solutions are explained in Ramabhadran et al [43] and Williams and Loyalka [11]. We have compared the DSMC results against the analytical results for all these test problems and test cases, and discussed the same later in this chapter.

5.4 Implementation of the DSMC Technique

For our simulation here, we use 100,000 particles as the initial particle population. All the test problems simulated and presented in this chapter assume a single component (water), to be present in all the particles. As explained in the test problems in the earlier chapters, here too, these particles have their particle diameters ranging from 0.01 μm to 20 μm. For display purposes, there are 20 sections considered which are logarithmically spaced in particle diameters. For all the test problems, the initial particle size distribution is assumed to follow a logarithmic distribution and the individual particle diameters of these 100,000 particles present initially are sampled from this distribution.

The total component mass of all the particles present initially is assumed to be in the order of 10^{-19} kg with the particle size following a logarithmic distribution. All the particles are assumed to be made of only one component – water, with density, ρ = 1,000

kg m^{-3}. This results in the initial total volume of particles, ϕ_0 to be in the order of 10^{-17} m^3 and the average initial particle volume, v_0 to be in the order of 10^{-22} m^3.

5.4.1 Test Problem I: Condensation

This test problem includes only the condensation process. The time intervals are progressively reduced until good accuracy (convergence) is achieved, and the results reported correspond to an approximately small interval. The mass condensed on each particle, $\tilde{u}(d_p, \Delta t)$ during the time interval, Δt for the two cases – I and II considered, are calculated as shown in equations (5-11) and (5-12), where d_p refers to the diameter of the particle (m), and σ_0 is the condensation rate constant (m^3 s^{-1}) for case I, and σ_1 is the condensation rate constant (s^{-1}) for case II. Also, note that the condensate mass, $\tilde{u}(d_p, \Delta t)$ is expressed in units of mass, kg.

$$Case\ I: \quad \tilde{u}(d_p, \Delta t) = \sigma_0\ \Delta t\ \rho \tag{5-11}$$

$$Case\ II: \ \tilde{u}(d_p, \Delta t) = \frac{\pi}{6} d_p^3\ \sigma_1\ \Delta t\ \rho \tag{5-12}$$

Once the initial conditions are set, condensation is allowed to occur where the mass condensed on each particle during the time interval, Δt is calculated using equation (5-11) for case I and equation (5-12) for case II. The condensate mass, $\tilde{u}(d_p, \Delta t)$ is then added to the mass of each particle. The particle number and volume distributions are then observed. This process is repeated until the end of the simulation.

5.4.2 Test Problem II: Condensation and Coagulation

This test problem includes both condensation and coagulation. Here, too, the aerosol behavior is observed at regular time intervals. At every time interval, Δt, the mass condensed on each particle, is calculated, followed by the coagulation of particles. The mass condensed on each particle depends on the condensation rate – constant or volume dependent condensation rates. Here, again, equation (5-11) is used to calculate the mass condensed when the condensation rate is constant, $I = \sigma_0$ ($m^3\ s^{-1}$) and equation (5-12) is used to calculate the condensate mass when the condensation rate is volume dependent, $I = \sigma_1 v$ ($m^3\ s^{-1}$).

After condensation, the mass of each particle is increased by the condensate mass, $\tilde{u}(d_p, \Delta t)$, following which coagulation of particles occurs. After every particle collision (coagulation), the collision time or the time per collision, t_c (s), is calculated using equation (5-13) where n_i refers to the total number of particles before collision (m^{-3}), n_{i+1} refers to the total number of particles after collision (m^{-3}), K refers to the coagulation rate ($m^3\ s^{-1}$), and the factor 2 in the numerator eliminates the double counting of collisions occurring between two particles.

$$Time\ per\ collision,\ t_c = \left(\frac{n_i - n_{i+1}}{n_i n_{i+1}} \right) \frac{2}{K}\ ; \qquad n_{i+1} = n_i - 1 \tag{5-13}$$

The particles are allowed to coagulate until the total time of collisions is approximately equal to the time interval, Δt for which the condensation had occurred in the previous step. In the reactor environment, condensation and coagulation occur

simultaneously. Hence, both condensation and coagulation have been implemented for the same amount of time, Δt, but in a sequence instead of occurring simultaneously. This sequence is an approximation we have made. Since we are taking very fine time intervals, this approximation stands good.

We have implemented the DSMC technique so that condensation occurs first, followed by coagulation. This order can be changed depending on the method of programming or the nature of the problem. After the condensation and coagulation processes have been simulated for a time interval, the particles are sorted in the sections for reporting purposes. The same steps are repeated for further iterations until the end of the simulation.

For case II in the test problem II, where both the condensation and coagulation rate constants are assumed to be volume dependent, we need very short time intervals which are not feasible due to limitations of present-day computational resources. These finer intervals are needed for determining the mass condensed on each particle during the time interval, Δt. So, in order to reduce every interval, Δt, into N intervals, such that the time interval now becomes smaller, $\Delta t/N$, equation (5-12) has to be modified such that the total mass of each particle, $u(d_p, t_i)$, at time t_i, after allowing condensation for time interval, Δt is as shown in equation (5-14), where d_p refers to the diameter (m) of the particle before condensation (at time, $t_i - \Delta t$). Here, too, the unit of the total mass of each particle, $u(d_p, t_i)$ is in kilograms.

$$u(d_p, t_i) = \frac{\pi}{6} d_p^3 \, (1+\sigma_1 \, \Delta t / N)^N \, \rho \tag{5-14}$$

This results in a new expression for the condensate mass, $\tilde{u}(d_p, \Delta t)$ and is given in equation (5-15) where $u(d_p, t_i - \Delta t)$ refers to the mass of the particle prior to the start of the condensation process.

$$\tilde{u}(d_p, \Delta t) = u(d_p, t_i) - u(d_p, t_i - \Delta t) = \frac{\pi}{6} d_p^3 \, (1+\sigma_1 \, \Delta t / N)^N \, \rho - \frac{\pi}{6} d_p^3 \, \rho \qquad (5\text{-}15)$$

This expression for $\tilde{u}(d_p, \Delta t)$ can be used for case II in test problem I and also for cases I and II in test problem II, where the condensation rates are considered as volume dependent.

5.5 Results and Discussions

5.5.1 Test Problem I: Condensation

Figure 25 shows how the total volume varies as a function of time for the two test cases. The condensation rates considered for cases I and II are: $I = \sigma_0 = 1 \times 10^{-5}$ ($m^3 \, s^{-1}$) and $I = \sigma_1 v = 5 \times 10^{-1} \, v$ ($m^3 \, s^{-1}$), respectively. The total volume was observed for 50 seconds for test problem I, and the same for test problem II was observed for 25 seconds. The total volume calculated, both analytically and using the DSMC technique, is plotted against time for both the cases – I and II, and are shown in fig. 25.

The DSMC results obtained for cases I and II agree well with the analytical results. The thick, dark line indicates the DSMC results while the thin line represents the analytical results. Since the results agree very closely, the curves obtained for the DSMC and analytical results are indistinguishable.

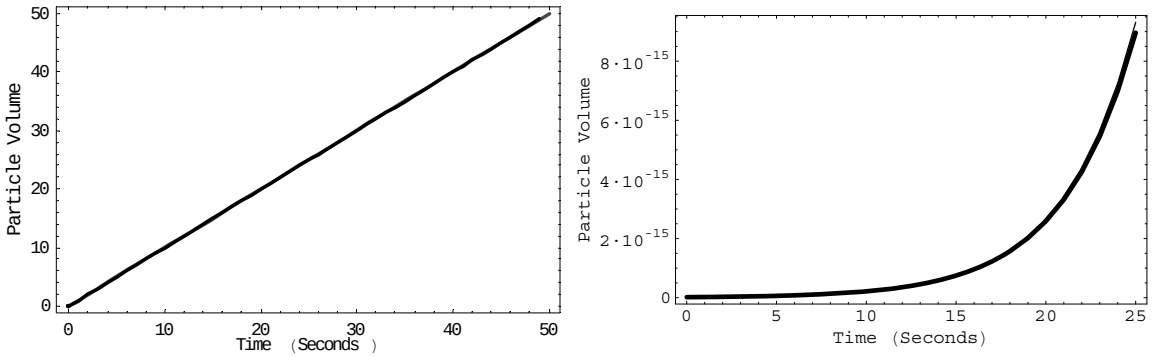

a) Case I: $\sigma_0 = 1 \times 10^{-5}$ ($m^3\ s^{-1}$) b) Case II: $\sigma_1 = 5 \times 10^{-1}$ (s^{-1})

Figure 25: DSMC vs. Analytical – A comparison.

5.5.2 Test Problem II: Condensation and Coagulation

The number of particles that undergo coagulation and the mass condensed were calculated at regular intervals. Since condensation was stronger in our examples, we allowed condensation to occur first followed by coagulation of particles for each interval. The particle number and total volume are observed for ~200 seconds for test cases I and III, and the same for test case II are observed for ~100 seconds. The number of particles remaining and total volume of particles present, both calculated analytically and using the DSMC technique, are plotted against time for each of the cases – I, II and III and are shown in fig. 26.

Figure 26: DSMC vs. Analytical – A comparison of results from test problem II.

Test Cases	Number vs. Time	Volume vs. Time
I: $K_0 = 5 \times 10^{-6}$ ($m^3\ s^{-1}$); $\sigma_1 = 2 \times 10^{-2}$ (s^{-1})	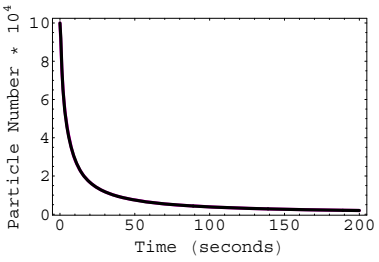	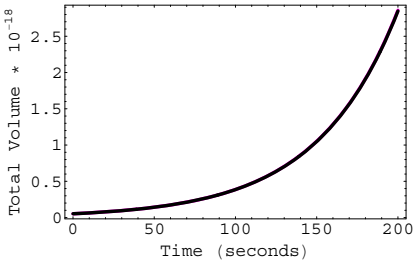
II: $K_1 = 5 \times 10^{-5}$ (s^{-1}); $\sigma_1 = 5 \times 10^{-1}$ (s^{-1})	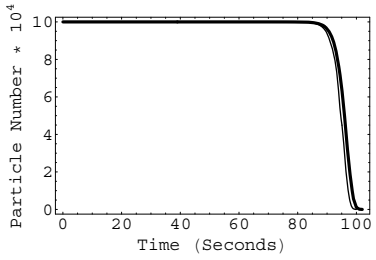	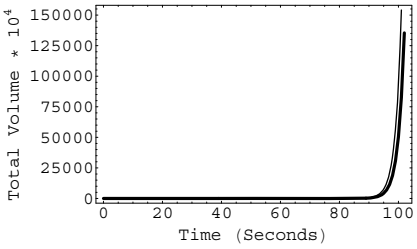
III: $K_0 = 5 \times 10^{-7}$ ($m^3\ s^{-1}$); $\sigma_0 = 1 \times 10^{-5}$ ($m^3\ s^{-1}$)	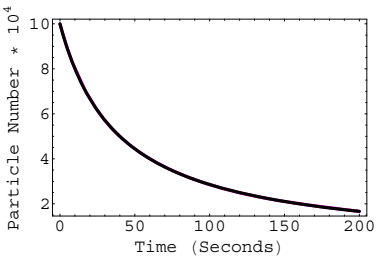	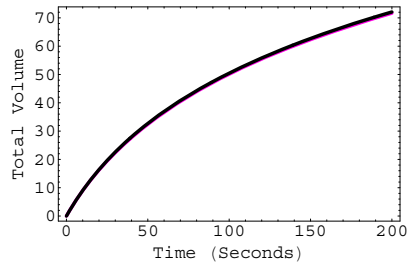

The dark thick lines indicate the DSMC results while the thin lines represent the analytical results. Since they agree very closely for cases I and III, the curves obtained for the DSMC and the analytical results are indistinguishable. The DSMC results obtained for cases I and III agree well with the analytical results. However, the DSMC result simulated for case II differs slightly from the analytical result. This is because the change in the distribution is very sharp, which poses a serious test of the simulation. It is possible to improve the agreement by using even finer time intervals than we have used. Again, we were not able to generate such fine time intervals due to the limitations of present day computer resources. The coagulation and condensation rates used for all three cases show that very strong condensation occurs in comparison to the coagulation process. These are shown clearly in figs. 31 and 32 later in this chapter.

5.5.3 Particle Number Distributions

We have also compared the DSMC results against the analytical results for the particle number distributions, $n(v,t)$ as a function of time, t, and particle size, v, for all the test cases. The results obtained for the two cases in test problem I and for different times, are shown in figs. 27a and 27b. The results obtained for the three test cases in test problem II and for different times are shown in figs. 28 – a, b and c. The thick gray lines in figs. 27 and 28 represent the analytical results while the thin black lines indicate the DSMC results. Since the DSMC results agree well with the analytical results, the thin black lines and the thick gray lines are indistinguishable.

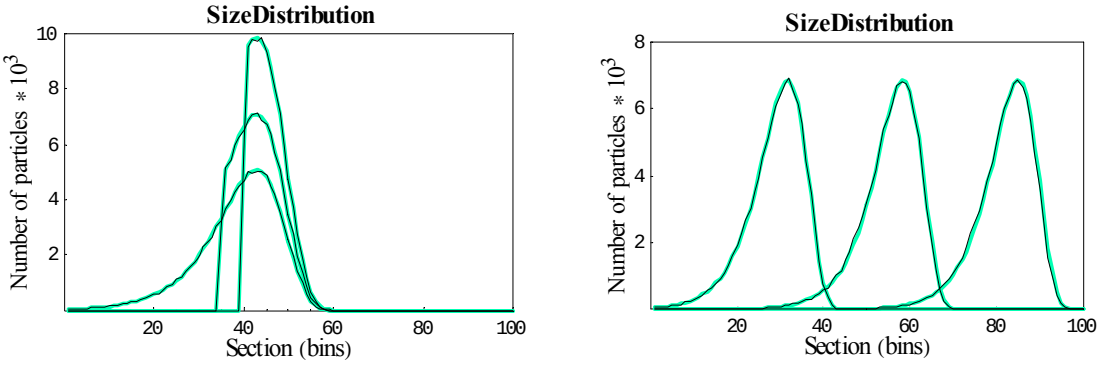

a) Case I b) Case II

Figure 27: Particle number distributions for test problem I.

(Thin black lines represent DSMC results and thick gray lines indicate analytical results)

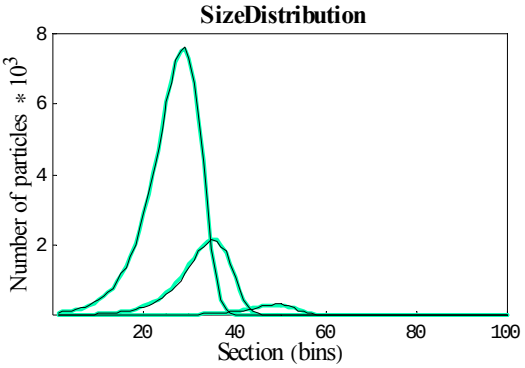

a) Case I: Constant coagulation and linear condensation rates.

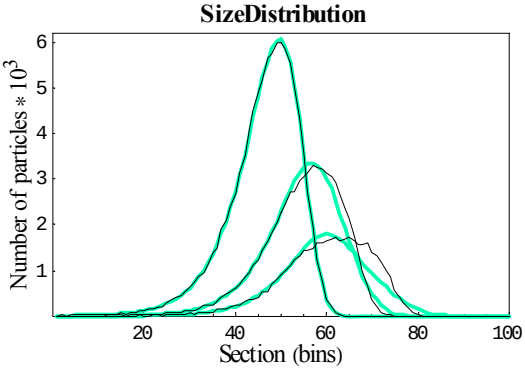

b) Case II: Linear condensation and coagulation rates.

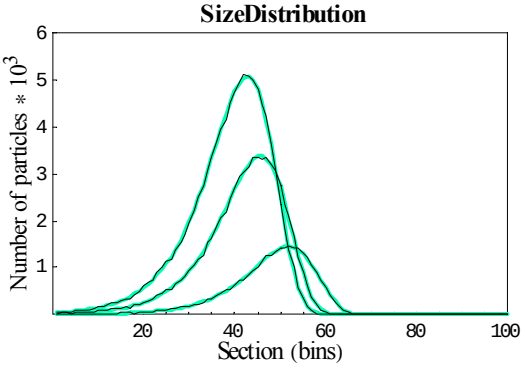

c) Case III: Constant condensation and coagulation rates.

Figure 28: Particle number distributions for test problem II.

(Thin black lines represent DSMC results and thick gray lines indicate analytical results)

The initial conditions considered for each of the test problems and corresponding test cases are specified in Table 14. The terms d_{min} and d_{max} refer to the minimum and maximum particle diameters (m). The abscissa represents 100 sections (bins) logarithmically spaced in particle diameters ranging from d_{min} to d_{max}. The particle population is shown in the ordinates. In order to check the time evolution of the particle size, the distributions were observed for three specific times for all the test problems simulated. The particle number distributions for the cases I and II of the condensation test problem I were observed for t = (0, 1500 and 10,000 seconds) and t = (0, 500 and 1300 seconds), respectively. The particle number distributions for cases I, II and III of the condensation and coagulation test problem II were observed for t = (0, 10 and 100 seconds), t = (0, 1200 and 1800 seconds) and t = (0, 1 and 10 seconds), respectively. Additionally, figs. 29 and 30 are provided to show the particle number distributions in a histogram format, obtained for test problems I and II and their corresponding test cases, at different times where the particle diameters are spaced in 20 sections (bins) for display purposes. The mean initial particle volume, the range of particle diameters, and the number of sections (bins) have been changed for this set of simulations and are given in Table 14. This change was necessary to show clearly the time evolution of particle sizes observed for the test problems.

Table 14: Initial conditions specified for the test problems and corresponding test cases.

Test Problems	Test Cases	I ($m^3\ s^{-1}$)	K ($m^3\ s^{-1}$)	v_0 (m^3)	d_{min} (m)	d_{max} (m)
I	I	10^{-25}	–	1.8×10^{-22}	1.0×10^{-8}	1.00×10^{-6}
	II	$10^{-2}\ v$	–	1.8×10^{-22}	1.0×10^{-8}	5.25×10^{-6}
II	I	$10^{-2}\ v$	5.0×10^{-6}	1.8×10^{-22}	1.0×10^{-8}	1.00×10^{-5}
	II	$10^{-3}\ v$	$1.0 \times 10^{6}\ (u + v)$	1.8×10^{-15}	2.5×10^{-7}	1.25×10^{-3}
	III	10^{-25}	5.0×10^{-6}	1.8×10^{-22}	1.0×10^{-8}	1.00×10^{-6}

Note: u and v are particle volumes (m^3).

Figure 29: Particle number distributions for test problem I.

Cases	Particle Number Distributions
I	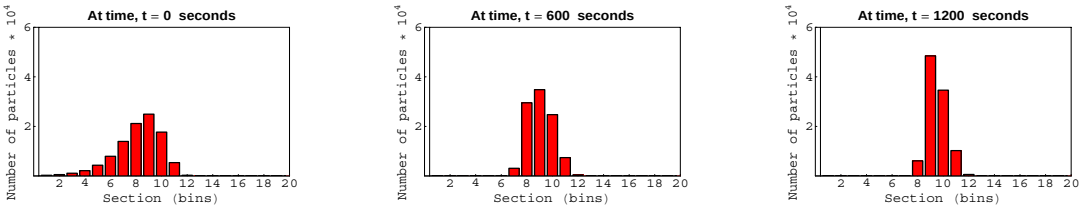
II	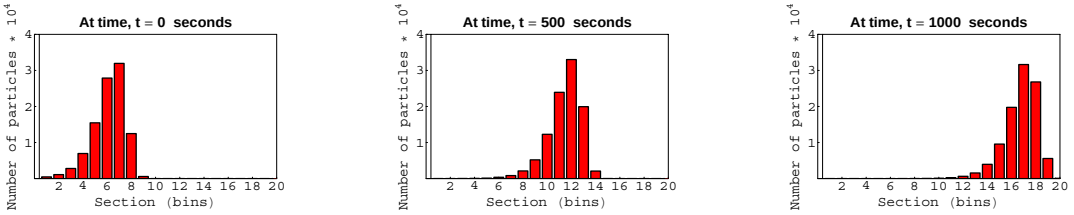

Figure 30: Particle number distributions for test problem II.

Cases	Particle Number Distributions
I	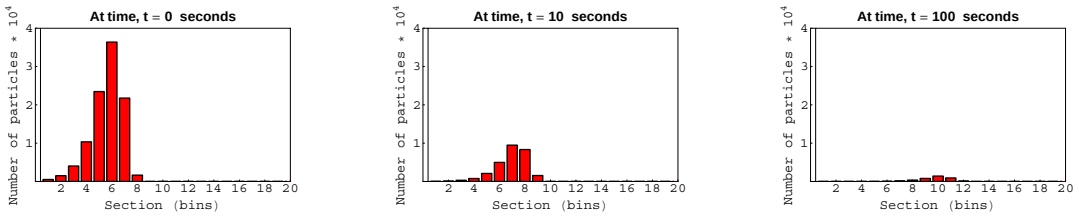
II	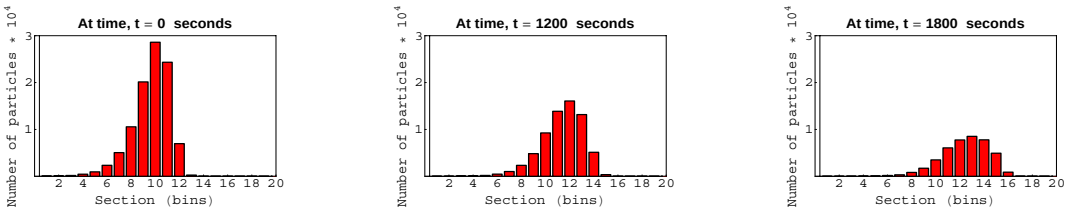
III	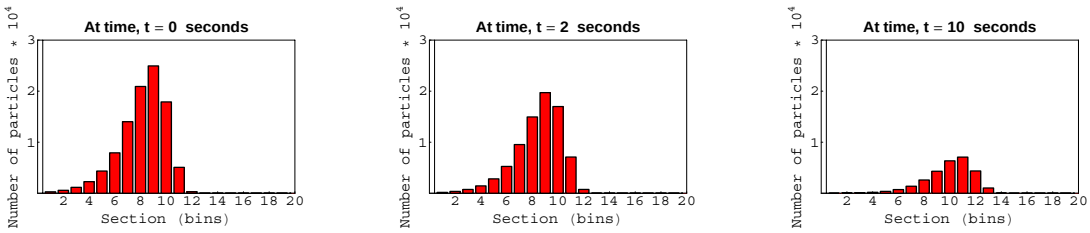

5.5.4 Effect of condensation and coagulation rates

In the case of constant coagulation and condensation rates, the particle number still depends only on the coagulation rate and hence, the condensation rate does not affect the particle number, as can be seen in Table 12 – case III. However, both the constant coagulation and condensation rates affect the total volume. For this reason, fig. 31 shows only the effect of constant coagulation and condensation rate constants on the total volume, $\phi(t)$ where the initial total volume of particles is in the order of 10^{-17} m^3. Figure 31a shows the plot obtained when using a specific coagulation rate constant, K_0 = 0.01 (m^3 s^{-1}) and varying the condensation rate constant, σ_0 as 0.001, 0.005 and 0.008, in units of m^3 s^{-1}. Figure 31b shows the effect of different coagulation rate constants, $K_0 = (0.05, 0.07, 0.1)$ m^3 s^{-1}, when the condensation rate constant is fixed at $\sigma_0 = 0.035$ m^3 s^{-1}. Figures 31a and 31b show that a small change in the condensation rate leads to a larger change in volume and also that coagulation has relatively less significant effect on the volume, $\phi(t)$.

In the case of linear coagulation and condensation rates, the total volume varies exponentially based on the condensation rate. But the particle number varies due to both the condensation and coagulation rates, as can be seen in Table 12 – case II. This is shown in figs. 32a and 32b. Figure 32 shows the effect of different coagulation and condensation rate constants on the particle number as a function of time. Figure 32a shows the effect of different condensation rate constants, $\sigma_1 = (0.025, 0.05, 0.019)$ s^{-1} when the coagulation rate constant is fixed at $K_1 = 0.5$ s^{-1}. Figure 32b shows the plot obtained when using the coagulation rate constants, K_1 = (0.01, 0.5, 1.0) s^{-1} and the

condensation rate constant, σ_1 = 0.035 s^{-1}. Here too, the initial total volume of particles considered is in the order of 10^{-17} m^3. Figures 32a and 32b reveal the dominant nature of the condensation rate on the particle number over the coagulation rate, as small variations in σ_0 leads to larger changes in the particle number. This is due to the increased mass condensed on each particle which increases the chances of coagulation, thereby reducing the total number of particles.

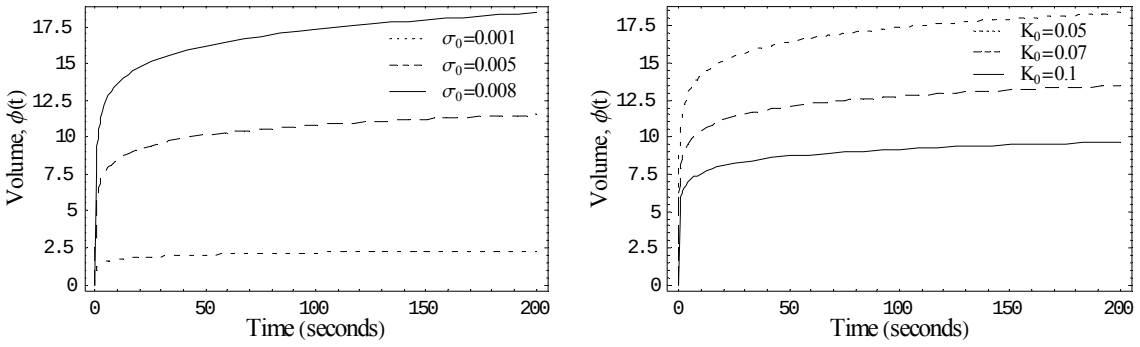

Figure 31: Effect of constant coagulation and condensation rates on total volume, $\phi(t)$.

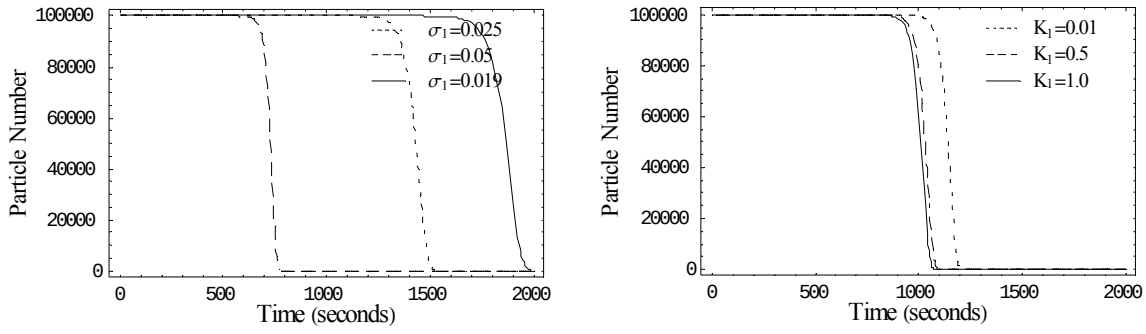

Figure 32: Effect of linear coagulation and condensation rates on particle number.

5.6 Multi-component Aerosol Condensation

In a real-time, post-accident reactor environment, several chemical species will be present. The high temperature and pressure conditions and the highly unstable situation might cause strong condensation to occur. Most of the chemical species present inside the containment might condense on existing aerosol particles. The mass condensed on each particle will then depend on several factors, such as the particle diameter, diffusion coefficient of the species (component) in air medium, and time. The condensate mass, $\tilde{u}_I(d_p)$ in units of kilograms, for each component, *I* over time, *t* can be calculated using the equation (5-16) [11, 16]:

$$\tilde{u}_I(d_p) = 2\pi D_I d_p \rho_I (S_I - 1) f\left(Kn_I\right) t \qquad and \qquad f\left(Kn_I\right) = \left[1 + \frac{\sqrt{\pi} Kn_I^2 \xi + \zeta}{Kn_I \xi + 1}\right]^{-1} \qquad (5\text{-}16)$$

where D_I is the diffusion coefficient of component, *I* in air in $m^2\ s^{-1}$, d_p is the diameter of particle, *p* in m, ρ_I is the saturation density of component, *I* in kg m^{-3} and is assumed to be 4% of the density at STP for water and 0.01% of the density at STP for all other components, S_I is the saturation ratio of component, *I* and is assumed to be 1.00374, Kn_I is the Knudsen number for component, *I* (dimensionless), and ξ and ζ are the dimensionless auxiliary factor and jump distance with values, 1.3333 and 1.0161 respectively [11]. Since, equation (5-16) resulted in a very large condensation rate and hence, condensate mass - $\tilde{u}_I(d_p)$, we introduced a factor of 10^{-9} in all our simulations such that the particle growth and evolution is observable.

5.7 Two-component, Aerosol Dynamics Test Problems: Coagulation, Deposition, Condensation and Source Reinforcement

After benchmarking our DSMC results against analytical results for a single component, condensation, and coagulation problem, we integrated all the four processes studied so far – coagulation, deposition, condensation and source reinforcement. Here, too, we assumed all the four processes to occur simultaneously, and are simulated in a sequence for the same time interval, Δt. Three test problems are simulated using the DSMC technique for a two-component aerosol dynamics problem undergoing coagulation, deposition, condensation and source reinforcement. The three test problems differ in the two-components used for the simulation. The components used in each test problem and their diffusion coefficients are given in Table 15. The initial conditions for the three test problems are the same and are similar to the initial conditions specified for test problem III in chapter 4. These initial conditions are explained as follows.

Table 15: Components used for test problem, I – III and their properties.

Test Problem	Component	Symbol	Molecular Weight (amu)	Density (kg m^{-3})	$D_I \times 10^{-4}$ (m^2 s^{-1})
I	Uranium Oxide	UO_2	270	10,970	0.12[a]
	Water	H_2O	18	1,000	0.24[b]
II	Water	H_2O	18	1,000	0.24
	Polonium	Po	218	9,196	0.056[c]
III	Water	H_2O	18	1,000	0.24
	Iodine	I_2	253	4,940	0.053[d]

[a] See Appendix for formula used [9, 48, 49] and calculations.
[b] Reference [9].
[c] Reference [50, 51].
[d] Reference [52].

For all three test problems, we considered particle diameter ranges between 0.01 and 20 microns and the sections (bins) used for display purposes total up to 20 bins, logarithmically spaced in particle diameters. The total mass concentration present initially is obtained from equation (3-6) as, $1.5 \times 10^{-10} \times M_I$. This accounts for ~100,000 particles. The new particles added to section 1 consist of component 2 alone and have a total mass concentration of $1.0 \times 10^{-18} / I^2$ kg m^{-3}, where I refers to the component being added. Due to very strong coagulation and condensation, we have introduced a scaling factor to reduce the coagulation and condensation rates by a factor 10^8 and 10^{-9} respectively, such that the aerosol behavior and evolution can be studied closely. Here, too, the diameters of the particles added are assumed to follow an arithmetic progression.

The particle number and component mass distributions are observed initially and at regular intervals of time for the three test problems and are shown in figs. 33 and 34. Figures 33 and 34 show the time evolution of the component mass and particle number distributions respectively. Also, it could be seen that the results for test problems II and III seem similar while the results for test problem I differ significantly. This is due to the effect of different component densities on the aerosol evolution and dynamics.

Figure 33: Component Mass Distributions at different times for test problems I – III.

Test Problem I: UO_2 and H_2O	Test Problem II: H_2O and Po-218	Test Problem III: H_2O and Iodine
Time: 0 seconds 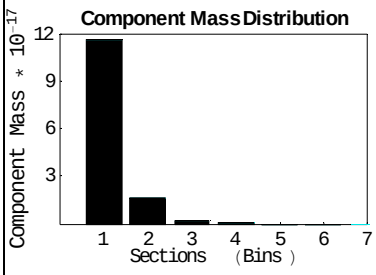	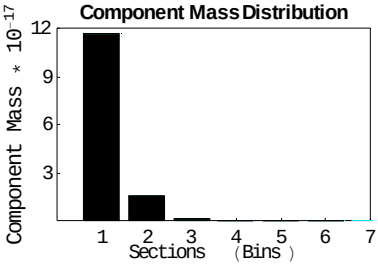	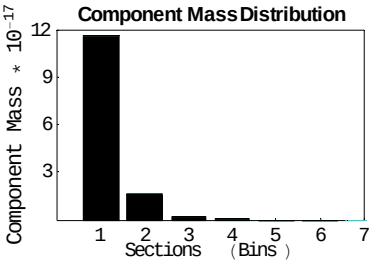
After 50 seconds, 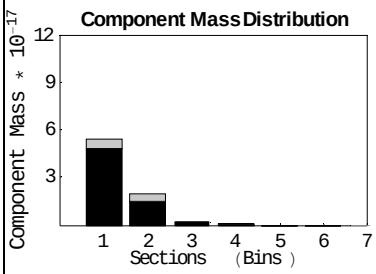	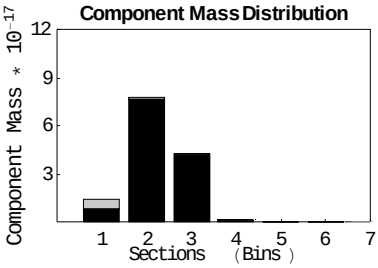	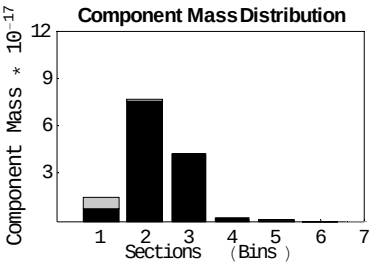
After 100 seconds, 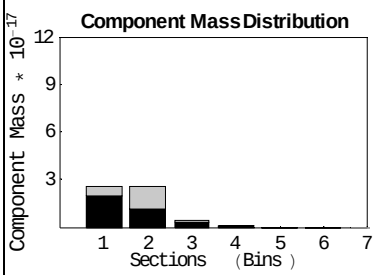	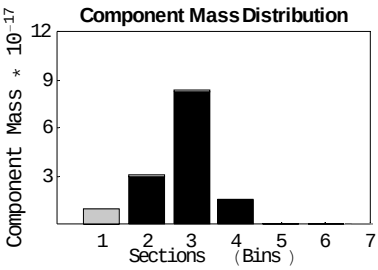	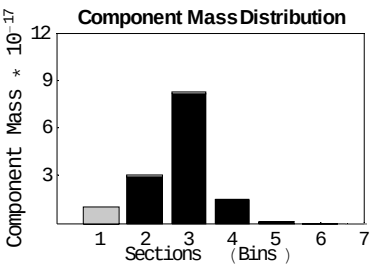
After 150 seconds, 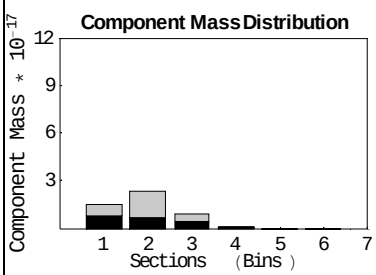	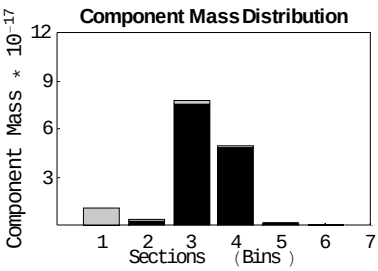	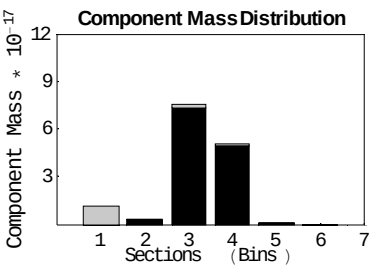

After 200 seconds,

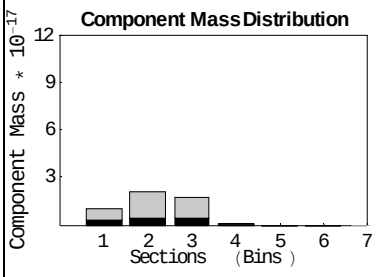

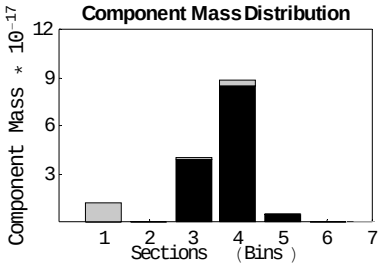

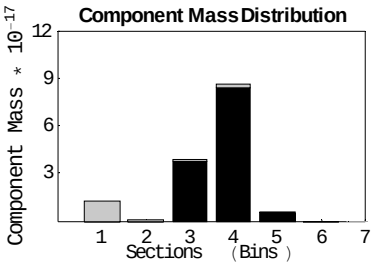

After 250 seconds,

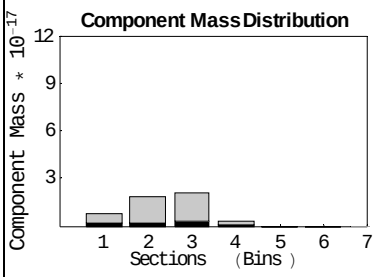

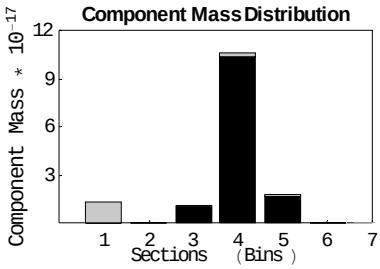

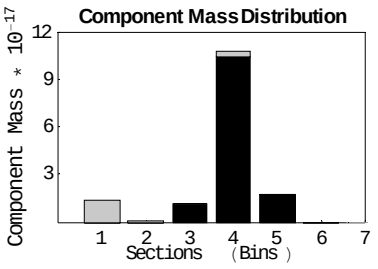

After 300 seconds,

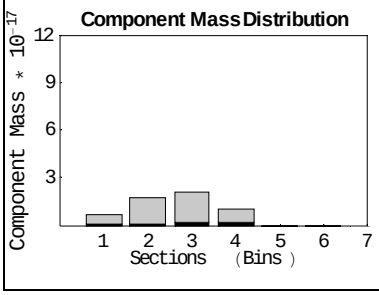

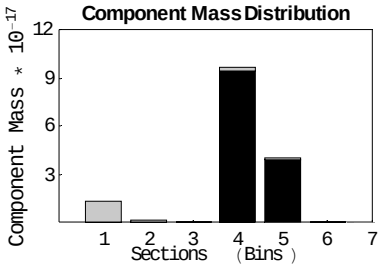

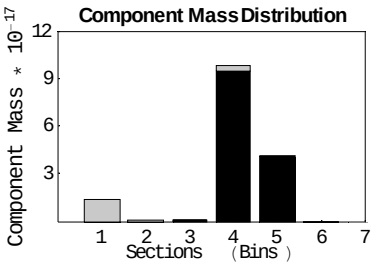

Figure 34: Particle Number Distributions at different times for test problems I – III.

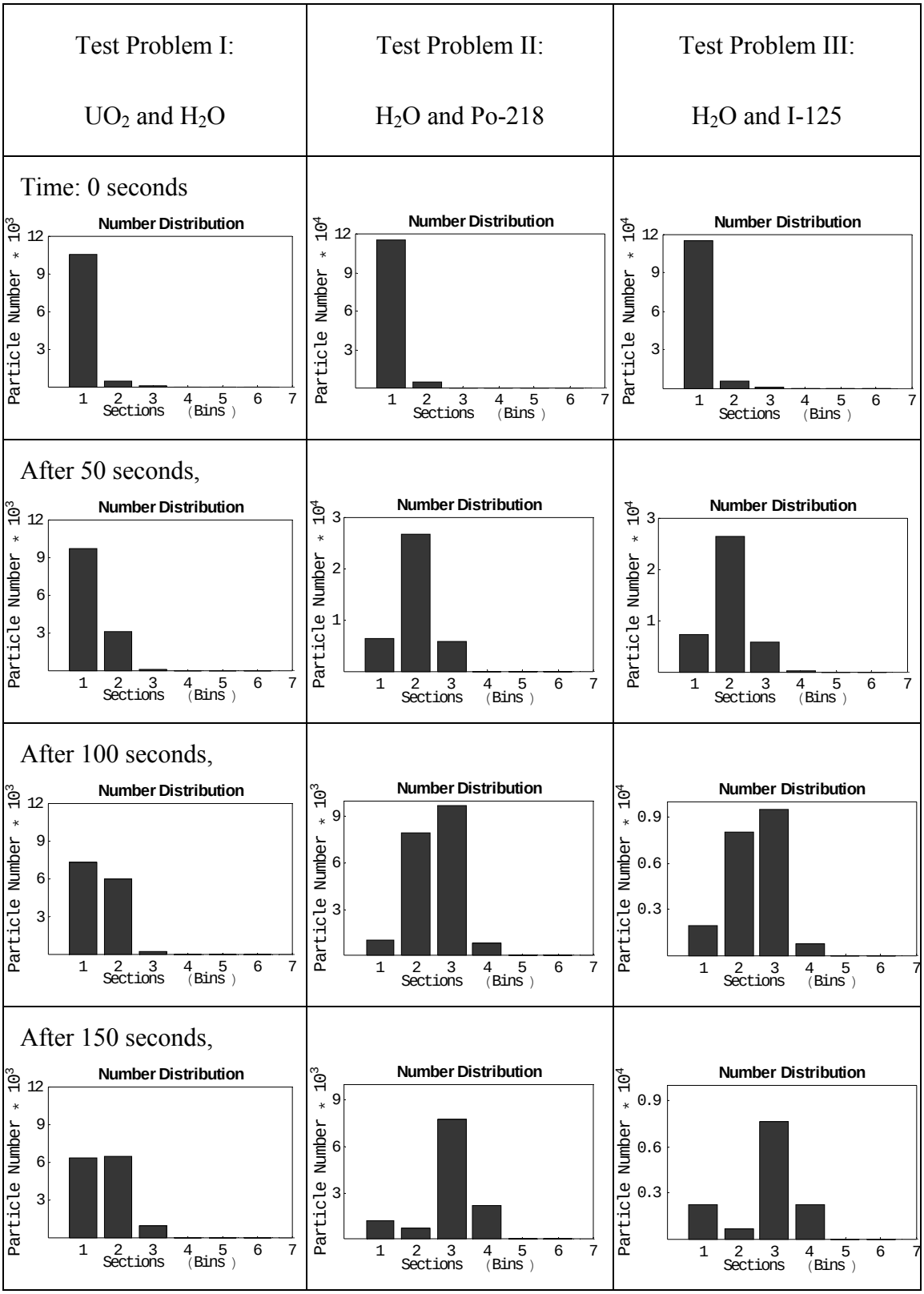

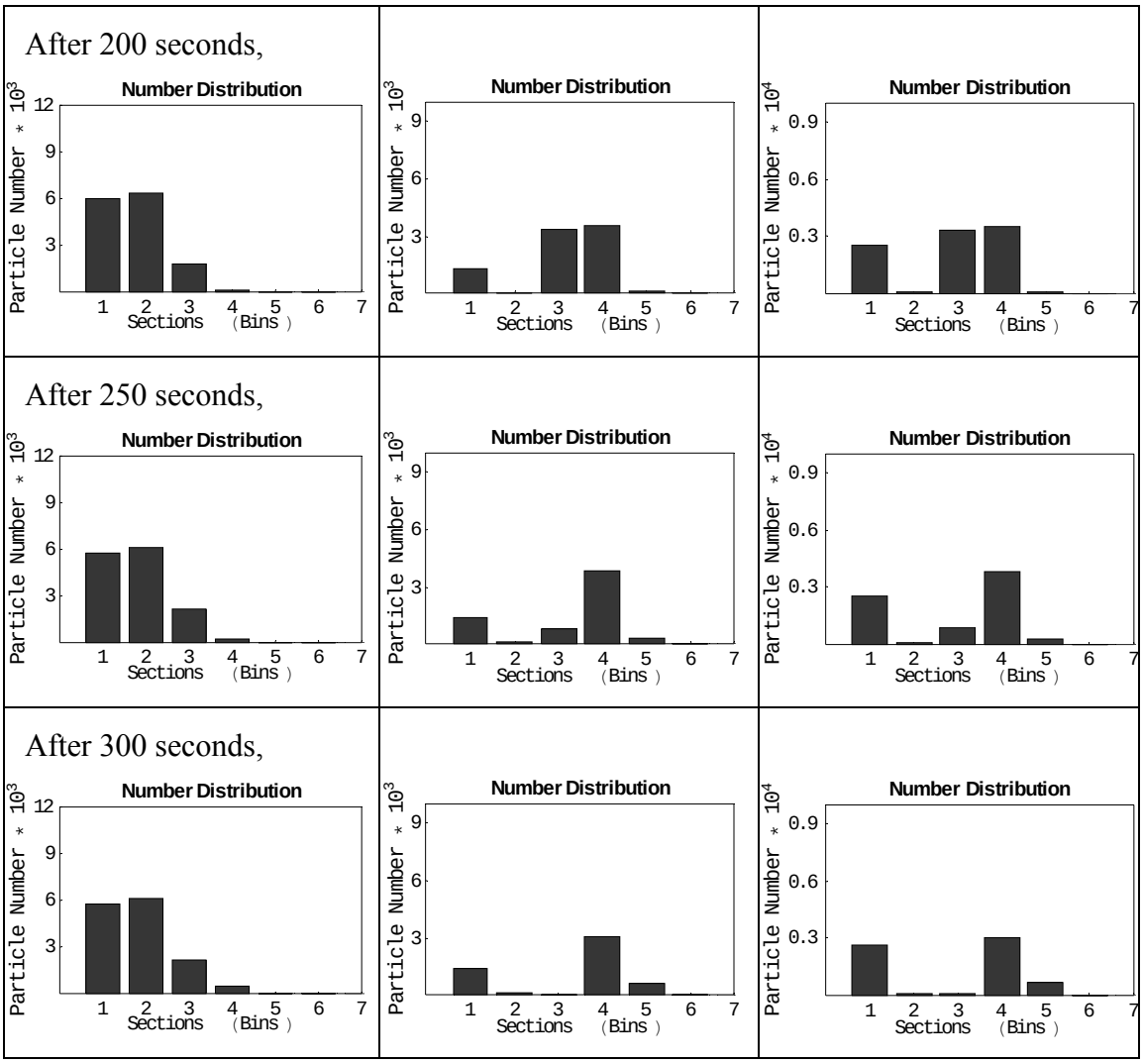
After 200 seconds,
Number Distribution
Particle Number * 10^3
Sections (Bins)
Number Distribution
Particle Number * 10^3
Sections (Bins)
Number Distribution
Particle Number * 10^4
Sections (Bins)
After 250 seconds,
Number Distribution
Particle Number * 10^3
Sections (Bins)
Number Distribution
Particle Number * 10^3
Sections (Bins)
Number Distribution
Particle Number * 10^4
Sections (Bins)
After 300 seconds,
Number Distribution
Particle Number * 10^3
Sections (Bins)
Number Distribution
Particle Number * 10^3
Sections (Bins)
Number Distribution
Particle Number * 10^4
Sections (Bins)

6. CONCLUSION

The purpose of this research had been to overcome the limitations of and eliminate use of assumptions made in the present-day computer codes and eventually develop a production computer program to predict and evaluate the dynamics and behavior of aerosols without compromising the physics of collisions. We approached the goal in steps – firstly, we included aerosol processes such as coagulation, deposition, condensation, and source reinforcement; secondly, we explored collision sampling algorithms in order to reduce computational overheads and hence, speed up computations; and finally, we explored the effect of different component densities on the dynamics of multi-component aerosols. Further research is required to explore several other factors such as shape, charge, radioactivity and spatial inhomogeneity.

We have explored several collisional sampling algorithms – direct sampling, the Metropolis sampling, the NTC method and modified direct sampling algorithms. We were able to verify the applicability of the Metropolis, the NTC and modified direct sampling algorithms to a collisional problem by comparing their distributions against that obtained using the direct sampling algorithm. We concluded that the Metropolis sampling algorithm gave better results than other sampling algorithms and also reduced the computation time significantly. Therefore, we were able to increase the total number of

particles considered for the study to 100,000 particles. By increasing the system memory to 2 GB (RAM), we were able to increase the initial particle population to 4 million.

We have extended the aerosol dynamics problem to include several aerosol processes such as deposition, coagulation and source reinforcement. We have simulated several test problems and compared the DSMC results against the sectional and analytical results for appropriate test problems. The DSMC results agreed well with the analytical results simulated for test problems undergoing deposition in the presence and absence of aerosol coagulation. We were able to integrate coagulation, deposition and source reinforcement processes for multi-component aerosol dynamics problem, and simulated several test problems with different particle compositions.

We further simulated three test problems to study the effect of different component densities on the aerosol dynamics problem. From our results, we concluded that the assumption of a single mean density for a multi-component aerosol dynamics problem leads to results that are not in agreement with the actual physics of the problem.

Further, we extended the study to explore aerosol condensation for a challenging single component problem. We were able to simulate the DSMC results for several test problems and test cases. A comparison on the DSMC results against the analytical results showed that the DSMC results were in excellent agreement with the analytical results, for all the test problems and test cases involving aerosol condensation and coagulation processes.

The aerosol condensation process implemented using the DSMC technique for a single component problem has been integrated with the aerosol dynamics to include

aerosol processes such as coagulation, deposition, condensation and source reinforcement, and also extended to study the multi-component aerosol dynamics problem. We have simulated three test problems with three different sets of components and the results presented illustrate the time evolution of the particle number and component mass distributions.

This research assumed a spatially homogeneous medium. But in real-time accident scenarios, the medium under study will be heterogeneous in nature (spatially inhomogeneity). There is scope in future to study and account for the effects of spatial inhomogeneities in this research.

Furthermore, the particles (aerosols) considered in the current research have been assumed to be rigid spheres which may not hold good at all times. Hence, this work can be extended to consider the shape effects of the aerosols under study.

We should also note that simultaneous work is being performed in exploring the effects of charge and radioactivity on aerosol particles and their evolution and behavior. After completion of this study, their work can also be integrated with the current study to make a more complete model to explore the dynamics of multi-component aerosols without compromising the collisional physics.

At every stage of the development of this research, a simultaneous effort should be made to explore acceleration schemes, overcome computational overheads (limitations) and also, improve the speed of computations.

REFERENCES

1. U. S. Atomic Energy Commission, "Theoretical Possibilities and Consequences of Major Accidents on Large Nuclear Power Plants," Report # WASH-740 (1957).
2. U. S. Atomic Energy Commission, "Calculation of Distance Factors for Power and Test Reactor Sites," Report # TID-14844 (1962).
3. U. S. Department of Energy, "Health and Environmental Consequences of the Chernobyl Nuclear Power Plant Accident," Report # DOE/ER-0332, UC-41 & 48 (1987).
4. U. S. Nuclear Regulatory Commission, "Reactor Safety Study: An Assessment of Accident Risks in U.S. Power Plants," Report # WASH-1400, NUREG-75/014 (1975).
5. U. S. Nuclear Regulatory Commission, "Technical Basis for Estimating Fission Product Behavior During LWR Accidents," Report # NUREG-0772 (1981).
6. U. S. Nuclear Regulatory Commission, "Severe Accident Risks: An Assessment for Five U. S. Nuclear Power Plants," (Final Summary Report) NUREG-1150, Vols. 1-2 (1990).
7. Soffer, L., "Revision of Reactor Accident Source Terms and Implications for Nuclear Air Cleaning Requirements," 22nd DOE/NRC Nuclear Air Cleaning and Treatment Conference, Session 8: Reactor Accidents (1992).
8. Loyalka, S. K., "Mechanics of Aerosols in Nuclear Reactor Safety: A Review," Prog. Nuc. Energy, **12**, 1 (1983).

9. Hinds, W. C., Aerosol Technology: Properties, Behavior, and Measurement of Airborne Particles, John Wiley & Sons, New York (1982).
10. Friedlander, S. K., Smoke, Dust, and Haze: Fundamentals of Aerosol Dynamics, Oxford University Press, Oxford (2000).
11. Williams, M. M. R. and Loyalka, S. K., Aerosol Science: Theory and Practice with Special Applications to the Nuclear Industry**,** Pergamon Press, Oxford, U. K. (1991).
12. Kress, T. S., "Review of the Status of Validation of the Computer Codes Used in the Severe Accident Source Term Reassessment Study," (BMI-2104), ORNL-2104, Oak Ridge, Tennesse 37831 (1985).
13. Gelbard, F., "MAEROS User Manual," NUREG/CR-1391, SAND80-0822, Sandia National Laboratories, Albuquerque, New Mexico (1982).
14. Allison, C., Rest, J., Lorenz, R., Hagrman, D., Carlson, E., and Broughton, J., "Severe Core Damage and Associated In-vessel Fission Product Release," Prog. Nuc. Energy, **20**, 89 (1987).
15. Brockmann, J. E., "Ex-vessel Releases: Aerosol Source Terms in Reactor Accidents," Prog. Nuc. Energy, **19**, 7 (1987).
16. Park, J. W., "Solutions of Aerosol GDE for ReactorSafety," Ph. D. Thesis, University of Missouri – Columbia (1988).
17. "CONTAIN 1.2 Code Manual, A Computer Code for Severe Accident Analysis," Sandia National Laboratories, Albuquerque, New Mexico. Prepared for the U. S. Nuclear Regulatory Commission (1993).

18. Bixler, N., "VICTORIA 2.0: A Mechanistic Model for Radionuclide Behavior in a Nuclear Reactor Coolant System under Severe Accident Conditions" (1998).
19. Gauntt, R., "MELCOR Computer Code Manuals: Primer and User's Guide," Version 1.8.5, Rev.2, Vol. 1 (2000).
20. Loyalka, S. K., "Direct Simulation of Multi-component Aerosol Dynamics," Trans. American Nuclear Society, **88**, 334 (2003).
21. Rangaraj, D. and Loyalka, S. K., "Direct Simulation Monte Carlo Aerosol Dynamics II – Role of Component Density Difference in Brownian Agglomeration," Trans. American Nuclear Society, **90**, 301 (2004).
22. Palaniswaamy, G., and Loyalka, S. K., "Direct Simulation Monte Carlo Aerosol Dynamics: Coagulation and Collisional Sampling," Nucl. Tech., **156**, 29 (2006).
23. Bird, G. A., Molecular Gas Dynamics and Direct Simulation of Gas Flows, Oxford University Press, Oxford (1994).
24. Metropolis, N., Rosenbluth, A. W., Rosenbluth, M. N., Teller, A. H. and Teller, E., "Equation of state calculations by fast computing machines," J. Chem. Phys., **21**, 1087 (1953).
25. Palaniswaamy, G., and Loyalka, S. K., "Direct Simulation Monte Carlo Aerosol Dynamics: Collisional Sampling Algorithms," Ann. Nucl. Energy, **156**, 29 (2006).
26. Palaniswaamy, G., and Loyalka, S. K., "Direct Simulation Monte Carlo Aerosol Dynamics: Coagulation, Deposition, and Source Reinforcement," Nucl. Tech., (Accepted for publication in November, 2007 issue).

27. Fuchs, N. A., The Mechanics of Aerosols, Pergamon Press, New York, NY (1964).
28. Gelbard, F. M. and Seinfeld, J. H., "Simulation of Multi-component Aerosol Dynamics", J. Colloid Interface Sci., **78**, 485 (1980).
29. Fuchs, N. A., and Sutugin, A. G., "High Dispersed Aerosols," in Topics in Current Aerosol Research, Vol. 2, G. M. Hidy and J. R. Brock, Eds., Pergamon Press, Oxford, U. K. (1971).
30. Bird, G. A., Molecular Gas Dynamics, Oxford University Press, Oxford (1976).
31. Saffman, P. G., and Turner, J. S., "On the Collision of Drops in Turbulent Clouds," J. Fluid Mech, **1**, 16 (1956).
32. Loyalka, S. K., "Brownian Coagulation of Aerosols," J. Colloid Interface Sci., **57**, 3 (1976).
33. Buckley, R. L. and Loyalka, S. K., "Implementation of a New Model for Gravitational Collision Cross Sections in Nuclear Aerosol Codes," Nucl. Tech., **109**, 346 (1995).
34. Koonin, S. E., Computational Physics, The Benjamin/Cummings Publishing Company Inc., California, USA (1986).
35. Robert, C. P. and Casella, G., Monte Carlo Statistical Methods, 2nd Edition, Springer, New York (2004).
36. Mathgroup forums on Mathematica website. (Accessed on 02/06/2007). Web address: http://forums.wolfram.com/mathgroup/archive/1995/Jul/msg00211.html.

37. Prieve, D. C., and Ruckenstein, E., "Rates of Deposition of Brownian Particles Calculated by Lumping Interaction Forces into a Boundary Condition," J. Colloid Interface Sci., **57**, 547 (1976).

38. Fernandes, A., and Loyalka, S. K., "Modeling of Thermophoretic Deposition of Aerosols in Nuclear Reactor Containments," Nucl. Tech., **116**, 270 (1996).

39. Fernandes, A., and Loyalka, S. K., "Modeling of Diffusive Gravitational Aerosol Deposition in CONTAIN," Nucl. Tech., **113**, 155 (1996).

40. Park, J. W., and Loyalka, S. K., "Role of Spatial Inhomogeneities in Source Term Aerosol Dynamics," Nucl.Sci. & Engg.,**101**, 269-279 (1989).

41. Simons, S., "The Coagulation and Deposition of Radioactive Aerosols," Ann. Nucl. Energy, **8**, 287-194 (1981).

42. Corner, J., and Pendlebury, E. D., "The Coagulation and Deposition of a Stirred Aerosol," Proc. Phys. Soc. Lond., **B64**, 645-654 (1951).

43. Ramabhadran, T. E., Peterson, T. W., Seinfeld, J. H., "Dynamics of Aerosol Coagulation and Condensation," J. AIChe, **22** (5), 840 (1976).

44. Gelbard, F., and Seinfled, J. H., "Exact Solution of the General Dynamics Equation for Aerosol Growth by Condensation," J. Colloid Interface Sci., **68** (1), 173 (1979).

45. Park, J. W., and Loyalka, S. K., "Kinetic Theory of Gelation: Numerical Simulation and Comparison with Analytical Results," J. Colloid Interface Sci., **125** (2), 615 (1988).

46. Park, J. W., and Loyalka, S. K., "Aerosol Growth by Condensation: A Generalization of Mason's Formula," J. Colloid Interface Sci., **125** (2), 712 (1988).

47. Simons, S., "The Condensation, Coagulation and Deposition of a Multi-component Radioactive Aerosol," Ann. Nucl. Energy, **9**, 473-479 (1982).

48. Tompson, R. V., and Loyalka, S. K., "Chapman-Enskog Solution for Diffusion: Pidduck's Equation for Arbitrary Mass Ratio," J. Phys. Fluids, **30** (7), 2073 (1987).

49. Ronchi, C., Iosilevski, I. L., and Yakub, E. S., Equation of State of Uranium Dioxide: Data Collection, Springer, New York (2004).

50. NCRP, "Measurement of Radon and Radon Daughters in Air," Report # 97 (1988).

51. Kinsara, A. A., Loyalka, S. K., and Tompson, R. V., "Polonium-218 Deposition Measurements in a Straight Tube," Trans. American Nuclear Society", 65, 373 (1992).

52. Langmuir, I., "The Evaporation of Small Spheres," Phys. Rev., **12**, 368-370 (1918).

APPENDIX

Calculation of Diffusion Coefficient of UO_2 in air

Chapman-Enskog Approximation: [48]

$$D = \frac{4\beta}{3\pi n_2 \sigma_{12}^2}\left(\frac{2kT}{m_1}\right)^{1/2}\left[\frac{9}{64}\frac{\pi^{1/2}}{\beta}\left(1+\frac{1}{\beta^2}\right)^{1/2}\right] \quad (\mathrm{m^2\ s^{-1}})$$

where

$$\beta^2 = \frac{m_2}{m_1}$$

$$\sigma_{12} = \frac{1}{2}(\sigma_1 + \sigma_2)$$

where

k: Boltzmann's constant = 1.38×10^{-23} J K^{-1}.

T: Temperature in K = 300 K.

n_2: Number density of air in m^{-3} = 2.687×10^{25} m^{-3}.

m_1: Molecular weight of UO_2 in kg = 4.4847×10^{-25} kg (270 amu).

m_2: Molecular weight of air in kg = 4.8169×10^{-26} kg (28.97 amu).

σ_1: Molecular diameter of UO_2 in m = 3.74 Å = 3.74×10^{-10} m. [9]

σ_2: Molecular diameter of air in m = 3.70 Å = 3.70×10^{-10} m. [49]

Using all the above data, the diffusion coefficient of UO_2 in air was calculated as 0.12×10^{-4} m^2 s^{-1}.

VITA

Geethpriya Palaniswaamy received her high school education at Shri Nehru Vidyalaya Matriculation Higher Secondary School, Coimbatore, Tamil Nadu, India. She received her Bachelors in Electronics and Instrumentation Engineering from Government College of Technology (2002), and then, she was employed with D. E. Shaw India Software Private Limited where she worked on the development of a hedge fund management tool. She received her M.S in Nuclear Engineering from University of Missouri Columbia in July, 2005 and graduated with a Ph.D. in Nuclear Engineering from University of Missouri Columbia in July, 2007.